

# Designing illumination source for Near-field Scanning Optical Microscope

A Thesis

submitted to

Indian Institute of Science Education and Research Pune  
in partial fulfillment of the requirements for the  
BS-MS Dual Degree Programme

by

Prashant Dagale



Indian Institute of Science Education and Research Pune  
Dr. Homi Bhabha Road,

Pashan, Pune 411008, INDIA.

April, 2020

Supervisor: Prof. Sushil Mujumdar

© Prashant Dagale 2020

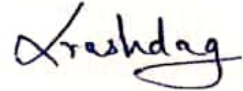
All rights reserved

# Certificate

This is to certify that this dissertation titled *Designing illumination source for Near-field Scanning Optical Microscope* towards the partial fulfilment of the BS-MS dual degree programme at the Indian Institute of Science Education and Research, Pune represents study/work carried out by Prashant Dagale at Tata Institute of Fundamental Research, Mumbai under the supervision of Prof. Sushil Mujumdar, Associate Professor, Department of Nuclear and Atomic Physics, TIFR, Mumbai during the academic year 2019-2020.



Prof. Sushil Mujumdar



Prashant Dagale

Committee:

Prof. Sushil Mujumdar

Dr. Bijay Kumar Agarwalla



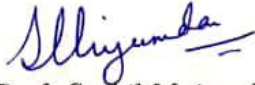


This thesis is dedicated to my parents and friends.

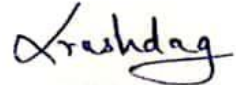


# Declaration

I hereby declare that the matter embodied in the report titled *Designing illumination source for Near-field Scanning Optical Microscope*, is the result of the work carried out by me at the Department of Nuclear and Atomic Physics, Tata Institute of Fundamental Research, Mumbai under the supervision of Prof. Sushil Mujumdar and the same has not been submitted elsewhere for any other degree.



Prof. Sushil Mujumdar



Prashant Dagale



# Acknowledgment

First and foremost, I wish to express my sincere gratitude to my supervisor, Prof. Sushil Mujumdar for providing me with an opportunity to work on my Master's Thesis in the Nano Optics and Mesoscopic Optics Laboratory(NOMOL) at TIFR, Mumbai. His firm commitment and dedication to resolve my doubts and understand the difficulties in conducting the experiments have helped me throughout the course of my stay at TIFR, Mumbai.

I also take this opportunity to express a deep sense of gratitude to all my lab members of NOMOL who have been there to train me in terms of values and hands-on experience. Particularly, I would like to thank Mr. Sreeman Kumar, whose knowledge and experience on Near-Field Scanning Optical Microscope (NSOM) has helped me numerous times. He has been a great mentor providing me with valuable inputs essential for my experiments. My colleagues, Sandip, Krishna, Rabisankar, Himadri and Deepak have been a great helping hand for solving all the issues in the laboratory to maintain the normal working standards of all instruments. They have also helped me in all scientific and non-scientific ways such as lending me their laptops, assisting me to help me move the optics from lab to lab, etc. Last but not the least, I thank all my IISER Pune - TIFR friends for making my stay memorable.



# Abstract

Near-field microscopy was invented to overcome the diffraction limit of the conventional optical microscopy. With the advent in nanostructures functional at optical wavelengths, such a device has become inevitable for studies in fundamental optics and photonics. Near-field microscopy captures the information contained in the evanescent waves to create high (subwavelength) resolution images. A major challenge in imaging subwavelength structures is the incoupling of excitation light. Free-space coupling is procedurally simple, but comes with the demerit of considerable unwanted scatter. The motivation for the project is to produce a guide for evanescent waves using a single-mode optical fiber. The evanescence sustained by the fiber can excite a sample in the Near-Field Scanning Optical Microscope (NSOM). This can circumvent substantial stray light in the imaging process. To serve this purpose, we obtained evanescent waves through micrometer thin optical fiber thread loop and coupled it to the samples. Characterisation and comparison of the incoupled light was done through the thin fiber loop and free space method. It was concluded that the incoupling of light using thin fiber loop offered high contrast and high signal to noise ratio optical signals in both near-field and far-field regimes.





# Contents

<b>Abstract</b>	<b>xi</b>
<b>1 Introduction</b>	<b>1</b>
1.1 Breaking the resolution limit . . . . .	1
1.2 Basics of evanescence . . . . .	3
1.3 Optical fibers . . . . .	5
<b>2 Source of evanescent wave</b>	<b>7</b>
2.1 Making of thin fiber thread . . . . .	7
2.2 Test for evanescence . . . . .	11
<b>3 Developing NSOM</b>	<b>17</b>
3.1 Fiber optic probes . . . . .	17
3.2 Shear Force Feedback . . . . .	19
<b>4 Investigation of NSOM and loop illumination</b>	<b>31</b>
4.1 Topographical scans . . . . .	31
4.2 Optical scans . . . . .	36
4.3 Loop illumination . . . . .	38



# Chapter 1

## Introduction

Near-field optical microscopy allows us to break the conventional far field limit [1,2] and attain resolution upto few nanometers [3]. An indigenous near-field scanning optical microscope (NSOM) is built to get highly resolved optical signals to investigate physics of nano-photonics. Conventional near-field optical microscopy involves raster scanning of samples using a sub-wavelength sized probe in close contact with the sample. The sample can be excited either by a source of evanescent waves or by far field light. At NOMOL, we study light propagation in photonic crystal(PhC) samples. These samples constitute of ordered structures of air holes in Gallium Arsenide(GaAs) membrane and this structure is further ingrained in GaAs brick. The infrared light can thus be coupled onto an edge of the brick and would propagate in it exciting the photonic crystal sample. Traditionally, the incoupling of light was done by free space coupling using beam focusing technique. Though being simple, it comes with the demerit of unwanted scatter over the sample leading to bad contrast and low signal to noise ratio. To overcome this effect we developed a low scatter evanescence source to illuminate the sample by coupling it onto the brick.

### 1.1 Breaking the resolution limit

The idea of excitation and collection of light in the near-field region was proposed by Edward Synge in 1928 [4]. This technique allows us to beat the far-field diffraction limit given by Ernst Abbe [5], which states that the minimum resolution( $l$ ) for an optical component is

limited by the spread of each image point due to diffraction and thus by its aperture size. The limit is given by Rayleigh's criterion [6] :

$$l = \frac{0.61\lambda}{\text{NA}} = \frac{0.61\lambda}{n\sin\theta_{max}} \quad (1.1)$$

where NA is numerical aperture of the optical component. It depends on the refractive index( $n$ ) of the surrounding medium and the maximum half-angle( $\theta_{max}$ ) of the light that enters or exits the component.

One can often relate the diffraction limit to Heisenberg's uncertainty principle [7]. From Figure 1.1 we observe that maximum transverse wavenumber is given as,  $\text{Max}(k_{\perp}) = \pm k\sin\theta_{max}$ . Hence, the spread in wavenumber can be defined as  $\Delta k = 2\text{Max}(k_{\perp}) = 4\pi\text{NA}/\lambda$ . Substituting this in equation 1.1 we have

$$\Delta x \Delta k = 0.61 \cdot 4\pi \quad (1.2)$$

which follows the uncertainty principle i.e the prouct is greater than 1/2.

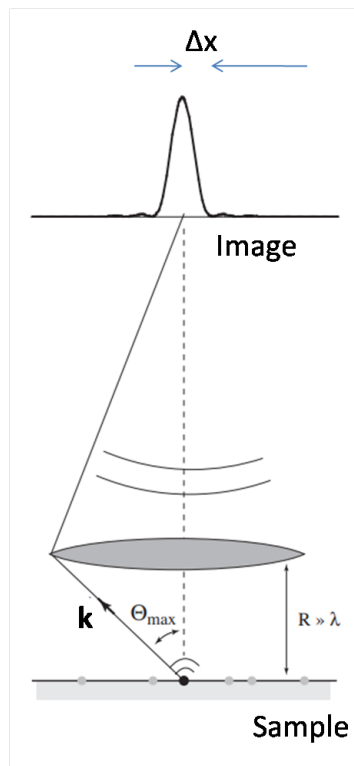


Figure 1.1: Schematic of diffraction limited microscope

In near field optics, the resolution dependence is not on the wavelength but on the aperture size or tip-diameter of the local probe [8]. Hence, the resolution limit mentioned above can easily be broken on having a probe-tip of diameter much smaller than the wavelength. The NSOM probe encapsulates the confined photon flux between the sample and the probe.

## 1.2 Basics of evanescence

Let us start with the theory of electromagnetic waves. The Maxwell's equation in homogeneous non-ferromagnetic medium is characterized by dielectric constant  $\epsilon$  and no source. So the wave equation for electric field is

$$\left( \frac{\partial^2}{\partial x^2} - \frac{\epsilon}{c^2} \frac{\partial^2}{\partial t^2} \right) \mathbf{E}(\mathbf{x}, t) = 0 \quad (1.3)$$

where  $\mathbf{E}(\mathbf{x}, t)$  is electric field at position  $\mathbf{x}$  and time  $t$  and  $c$  being the speed of light in vacuum. The solution to the wave equation is a plane wave:

$$\mathbf{E}(\mathbf{x}, t) = E_o e^{i\mathbf{k}\cdot\mathbf{x} - \omega t} \quad (1.4)$$

where  $n = \sqrt{\epsilon}$  is refractive index of the medium and  $\mathbf{k}$  is the wave vector pointing in the direction of wave propagation.

Consider a case where light is incident at the interface with two different media characterized by their different refractive indices. The solution of Maxwell's equation on one side does not extend to the other side and a complete solution is obtained by imposing boundary conditions and continuity arguments. At such interfaces, light is refracted and reflected so that we have incident and reflected wave in first medium( $n_1$ ) and refracted(transmitted) into second medium( $n_2$ ). Each of these waves is a plane wave and has the same form as equation (1.5) but with its own amplitude and wave-vector:

$$\begin{aligned} \mathbf{E}_I(\mathbf{x}, t) &= E_{oI} e^{in_1 \mathbf{k}_I \cdot \mathbf{x} - i\omega t} \\ \mathbf{E}_R(\mathbf{x}, t) &= E_{oR} e^{in_1 \mathbf{k}_R \cdot \mathbf{x} - i\omega t} \\ \mathbf{E}_T(\mathbf{x}, t) &= E_{oT} e^{in_2 \mathbf{k}_T \cdot \mathbf{x} - i\omega t} \end{aligned} \quad (1.5)$$

The wave vectors  $\mathbf{k}_I$ ,  $\mathbf{k}_R$  and  $\mathbf{k}_T$  for incident, reflected and transmitted, respectively are realized by the laws of reflection and refraction.

In this case, where light travels from a denser medium( $n_1$ ) into a rarer medium( $n_2$ ) with incidence angle( $\theta_I$ ), the light is refracted and the angle of refraction( $\theta_R$ ) is given by Snell's law

$$n_1 \sin \theta_I = n_2 \sin \theta_R \implies \cos \theta_R = \sqrt{1 - \frac{n_1^2 \sin^2 \theta_I}{n_2^2}} \quad (1.6)$$

The above equation holds only when the incidence angle( $\theta_I$ ) is less than the critical angle( $\theta_c$ ) given by :

$$\sin \theta_c = \frac{n_2}{n_1} \quad (1.7)$$

For  $\theta_I > \theta_c$ , equation 1.6 leads the angle of refraction to be a complex number

$$\cos \phi = i \sqrt{\frac{n_1^2 \sin^2 \theta_I}{n_2^2} - 1} = iA \quad (1.8)$$

where A is a real scalar. Thus for angle of incidence less than critical angle, light refracts into the rarer medium. However, for incidence angle greater than critical angle, total internal reflection (TIR) into the same (denser) medium takes place. This leads to the presence of incident and reflected wave and the transformation of transmitted wave to evanescent wave.

Consider the xz plane to be the plane of incidence such that xy plane would be the interface separating the two media. The three wave vectors have only x and z components, with no y component. The scalar product in the propagation term in the transmitted wave can be written as

$$in_2 k(x \sin \phi + z \cos \phi) = ikx n_1 \sin \theta - kzA \quad (1.9)$$

which then implies

$$\mathbf{E}_T(\mathbf{x}, t) = E_{oT} e^{-i\omega t} e^{ikx n_1 \sin \theta} e^{-kzA} \quad (1.10)$$

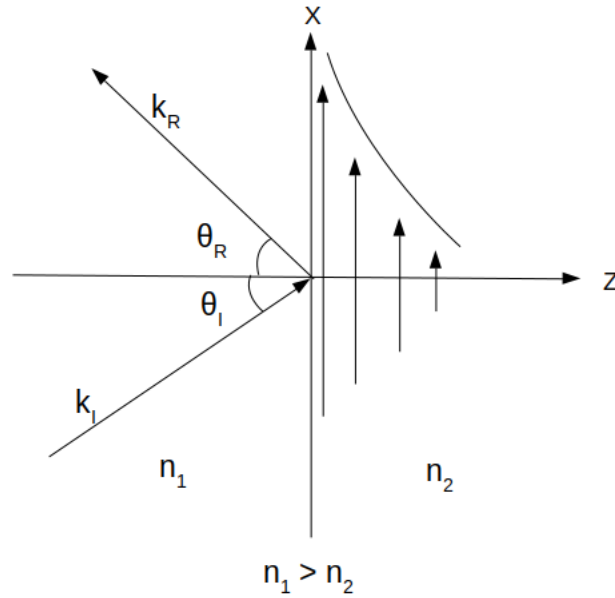


Figure 1.2: Schematic representation of evanescent wave.

The first and second term in the exponential are the standard terms as shown in equation (1.4) that represent the time dependent oscillatory behavior of  $\mathbf{E}$  and light propagation along the surface respectively. The third term, however, showcases the exponential decay of the amplitude of the electric field as a function of  $z$ . This type of electromagnetic wave whose amplitude is largest at the interface and decays exponentially away from the interface (as illustrated in Figure 1.2) is called an evanescent wave.

### 1.3 Optical fibers

An optical fiber is the key to high-speed, low-loss telecommunication technology where light is transmitted from one point to another over larger distances, higher bandwidths and with no electromagnetic interference. Transmission through optical fiber can be characterized in two ways: single mode, where light of a particular frequency is propagated and multi-mode, where broadband light propagates. The single mode optical fiber can be realized in terms of cylindrical waveguide in which light is transmitted via total internal reflection.

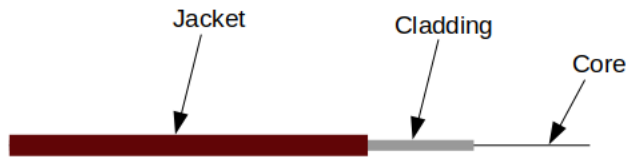


Figure 1.3: Components of an optical fiber.

An optical fiber consists of three main components:

- Core - The innermost part of fiber which typically has diameter of few micrometers( $\mu\text{m}$ ) for single mode and 50-100  $\mu\text{m}$  for multi-mode fibers. Generally it is made from silica with index-raising dopants such as  $\text{GeO}_2$ ,  $\text{P}_2\text{O}_5$  or  $\text{Al}_2\text{O}_3$ .
- Cladding - The material residing on top of core and has lower refractive index than core. It is also made from silica but fused with index-lowering dopants such as F or  $\text{B}_2\text{O}_3$ . Typical diameter is 150  $\mu\text{m}$ .
- Jacket - The polymer coating and the outermost layer of an optical fiber. It provides protective layer and robustness to the fiber.

Since the cladding has lower refractive index than the core, light encounters the core-cladding interface and undergoes total internal reflection. This process of TIR happens at every point of incidence hence allowing light to propagate throughout the fiber from one end to another. The core acts as a cylindrical waveguide for light transmission.



# Chapter 2

## Source of evanescent wave

As seen in section 1.2, at an interface exhibiting total internal reflection, evanescent waves are produced. Since light exhibits TIR at the core-cladding interface of an optical fiber, evanescent waves are formed. Hence we could use single mode optical fiber as a source of evanescent waves. But since the decay length of the evanescent waves is of the order of the wavelength, it decays into the cladding as its diameter is much larger than the decay length. Moreover, stripping the cladding of a single mode fiber is unfeasible. So we devised an experiment to get access to the evanescent light by obtaining thin optical fiber of about few micro-meter diameter. A circular loop of few millimeters diameter was made to get evanescent waves in all directions. This chapter reports the fabrication of thin fiber thread and confirmation of evanescent light from the thin fiber loop.

### 2.1 Making of thin fiber thread

Thin optical fiber thread is obtained by simultaneous melting and stretching the core-cladding part of the fiber. The CO<sub>2</sub> laser emission wavelength is approximately equal to the resonant wavelength of the SiO<sub>2</sub> lattice in glass, the material that the core and cladding is made of. The polymer jacket part is stripped off and the fiber is cleaned with methanol. The core-cladding is heated by exposing the stripped portion with the laser beam. This leads to its softening which thereafter is stretched using motorized micro-motion translational stage.

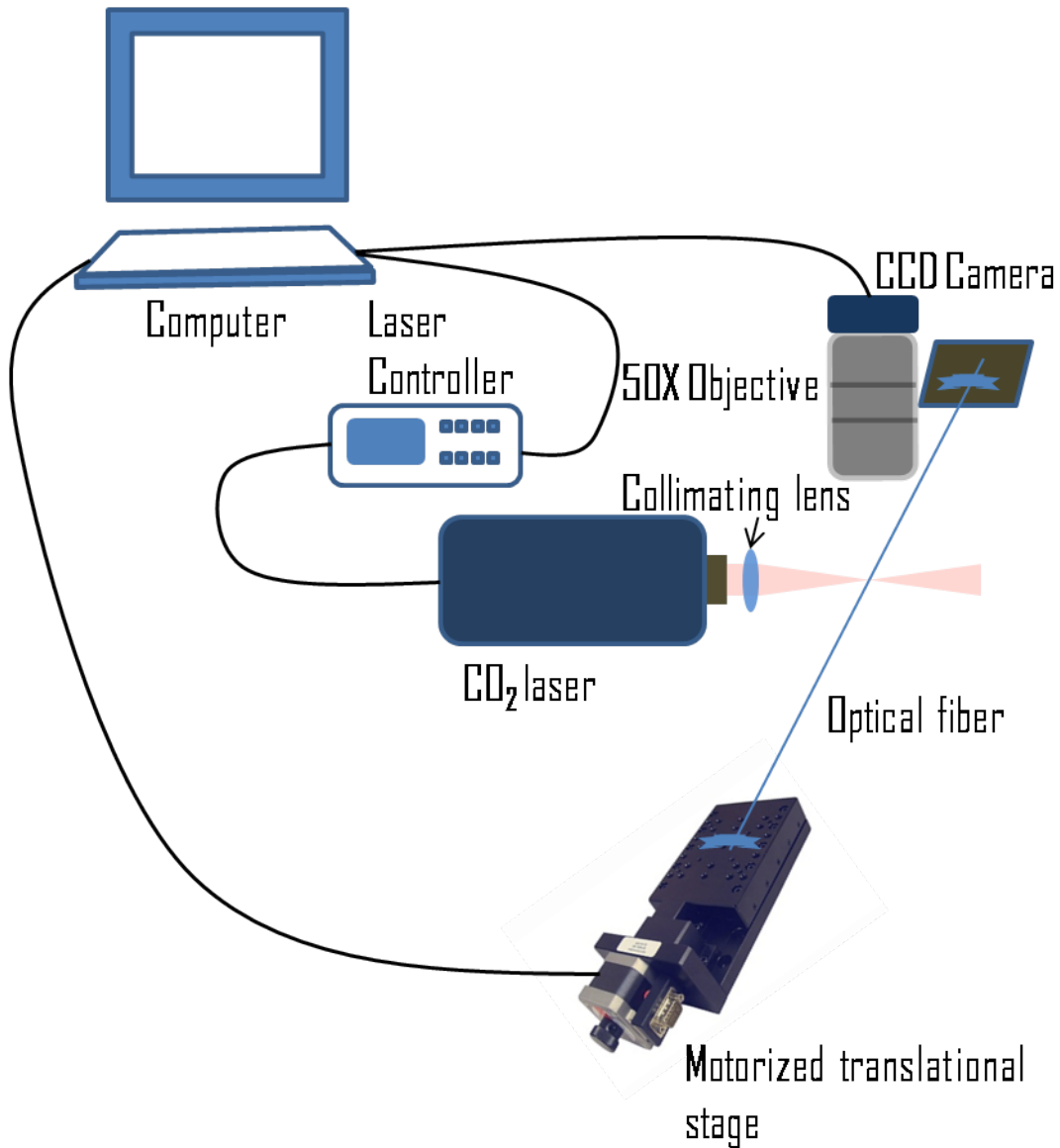


Figure 2.1: Schematic of experimental setup for obtaining thin fiber thread.

The experimental setup for making thin fiber thread (Figure 2.1) consists of the following components:

- CO<sub>2</sub> laser - Heat source to melt the optical fiber. Maximum attainable power is 10W
- Single mode optical fiber of 630nm.
- Micro-motion translational stage to pull the fiber at certain speed, maximum distance

and exposure for a delay time.

- CCD Camera to measure the thickness of the fiber thread by calibrating pixel size with cladding thickness.

We allow the fiber to be exposed to the high power CO<sub>2</sub> laser for a certain delay time. After the delay time, the translational stage pulls the fiber up to a fixed distance at a certain speed. This leads to formation of thin fiber thread of specific length and thickness. The thickness of the fiber thread was measured using the CCD image of the thread by calibrating the pixel size with the known thickness of fiber cladding. Typical values for the experimental variables and observations is shown in the following table (Figure 2.2).

Power (Duty Cycle)	Delay Time (sec)	Speed ( $\mu\text{m}/\text{sec}$ )	Move ( $\mu\text{m}$ )	Length (cm)	Thickness ( $\mu\text{m}$ )
0.600	15	370	9000	0.95	10.31
0.610	18	360	12000	1.25	7.43
0.625	20	370	14000	1.45	8.75
0.650	10	340	14000	1.50	6.25
0.675	5	370	15000	1.55	8.58
0.680	5	370	17000	1.75	6.31
0.700	5	370	17500	1.85	6.31

Figure 2.2: Observation table of experimental parameters .

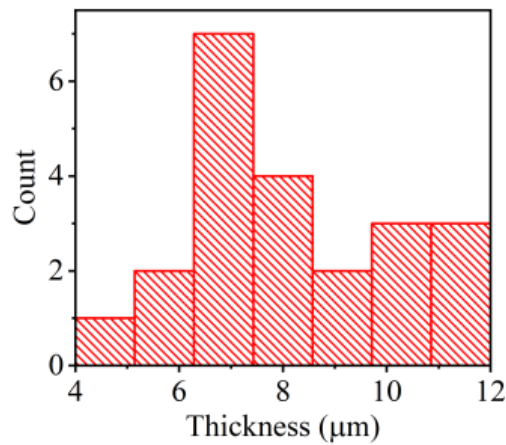


Figure 2.3: Histogram depicting fiber thread of varying thickness

Note that the thickness value recorded in the table is the thickness of the fiber thread at one end. The thickness is not completely uniform all over the length of the fiber. But since the non-uniformity is minute, the fiber thread obtained serves the purpose for us. Depending on everyday environmental changes in temperature, humidity, etc., the variables do not show a consistent trend and hence cannot be perfectly optimized for our desired configuration of thickness and length. We were able to prepare a total of 22 sample fiber threads and measure their thickness. Figure 2.3 shows the histogram of thickness for all the fiber samples prepared.

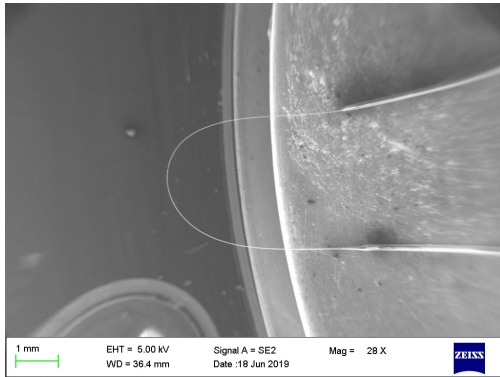


Figure 2.4: Fiber loop

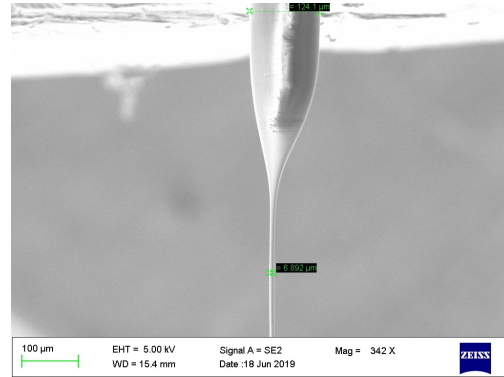


Figure 2.5: Fiber thread along with cladding

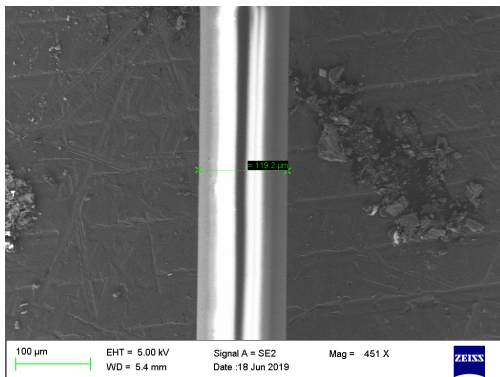


Figure 2.6: Cladding

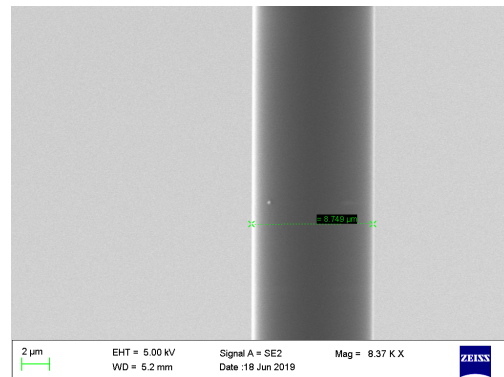


Figure 2.7: Fiber thread

Scanning Electron Microscopic(SEM) images of thin fiber thread of 7-9  $\mu\text{m}$  thickness and 1.2 cm length is shown in fig 2.4 - 2.7.

## 2.2 Test for evanescence

The thin fiber thread obtained was made into few millimeter diameter circular loop. Light was coupled to one end of the fiber such that light propagates through the thin fiber thread. Similar to the case of optical fiber, light propagation is governed by total internal reflection. The only difference being the two participating mediums. In thin fiber thread case, the two media are silica and air. Since evanescence exists at every such interface, forming a circular loop would give access to evanescent waves in wide range of directions (shown by red arrows in Figure 2.8) enabling ease of light coupling to the sample brick. An experiment was designed to verify the presence of evanescence by observing the illumination of samples in far field. It was done by coupling the evanescent light into the glass slide to illuminate scotch tape and polystyrene micro sphere samples.

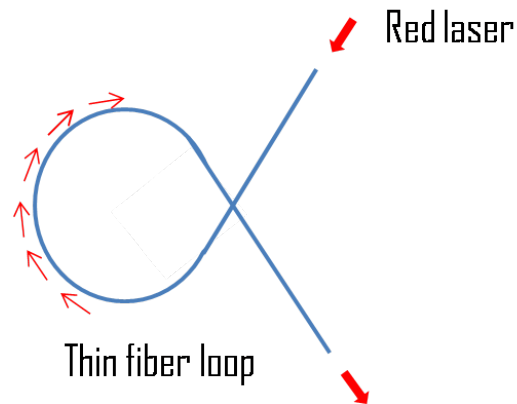


Figure 2.8: Schematic of evanescent wave vectors, shown by red arrows

### 2.2.1 Scotch tape illumination

To check for evanescence, a sample was prepared by pasting scotch tape on the side of a glass slide. Thin fiber thread loop was made and 630 nm light was passed through it. Using a translational stage, the loop was made to approach the other side of glass slide laterally such that the evanescent wave vector directs towards the tape sample. An imaging setup (Figure 2.9) was designed to detect light illumination of scotch tape sample.

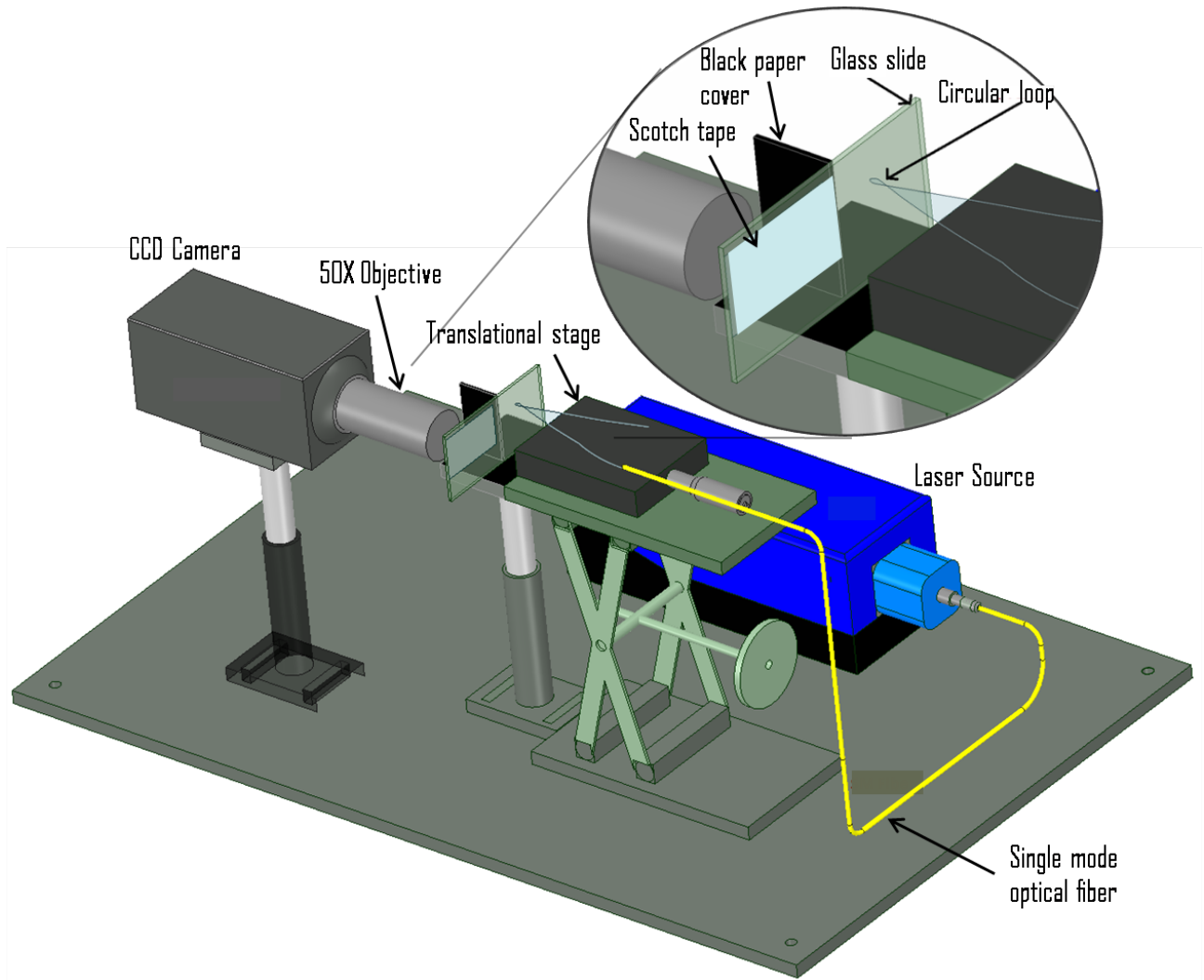


Figure 2.9: Scotch tape illumination setup

It was observed that taking the loop close enough to the glass slide resulted in the illumination of the scotch tape placed on the other end and side (Figure 2.10). The illumination is the result of coupling of evanescence from the thin fiber loop into the glass slide, consistent with wave vector matching condition. This phenomenon can be understood as an adaptation of frustrated total internal reflection. Hence the coupled wave propagates into the glass slide to the other end of slide illuminating the tape sample. A black paper cover was used to block the stray light from losses from the fiber thread to ensure that the tape sample is illuminated only by the coupled evanescent light.

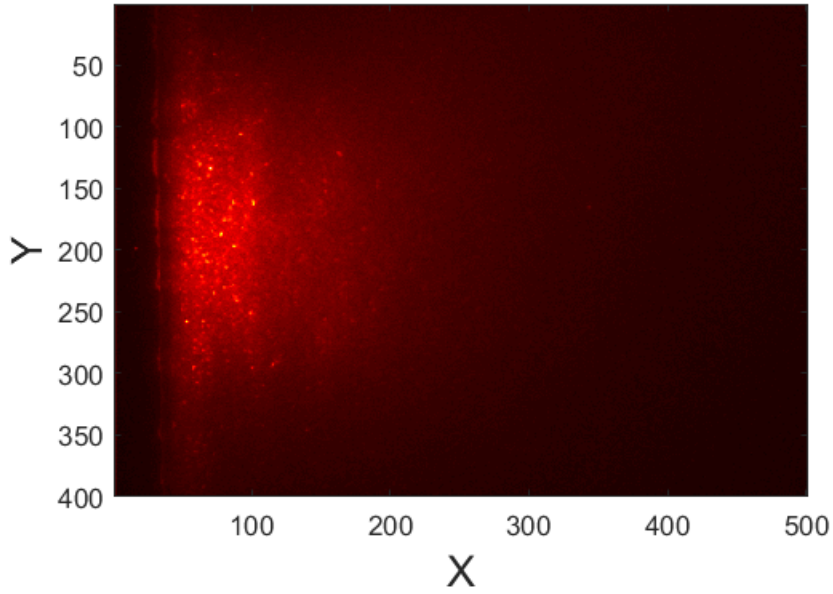


Figure 2.10: Far-field image of tape sample illumination

The intensity profile of tape illumination along x axis is plotted in Figure 2.10. Since the scotch tape is a diffusive medium we expect a decaying intensity profile. Thus, the decay length measured is  $2.34 \pm 0.03$  mm.

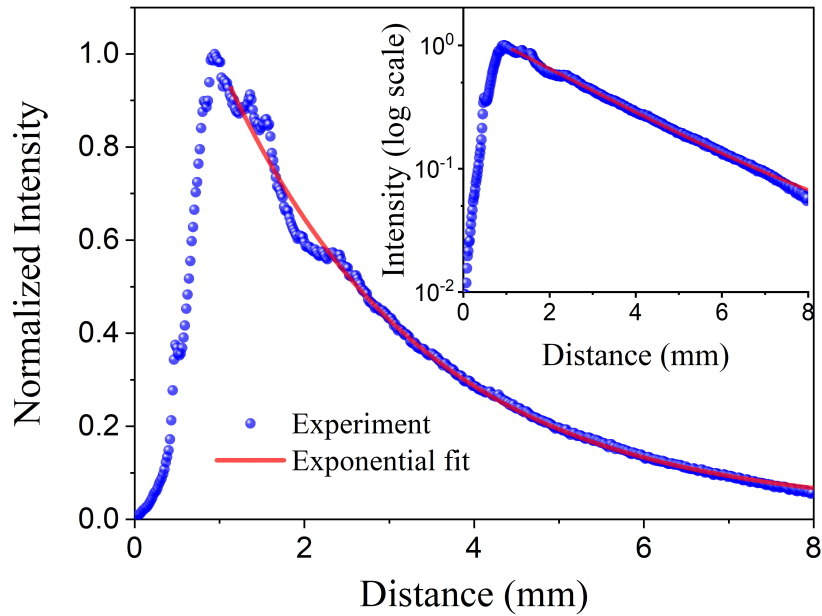


Figure 2.11: Intensity profile of tape sample illumination

### 2.2.2 Polystyrene sample illumination

An illumination setup was designed to simultaneously couple light into the glass slide by thin fiber loop and free space coupling method. The setup is similar to the earlier case (Figure 2.9) but with an additional free space beam coupled to the slide's edge and the scotch tape replaced with polystyrene microspheres. The mean diameter of these microspheres is  $1\mu m$ . This experiment allows us to compare the two methods of illumination by quantifying the extent of scatterers measured by the signal to background ratio,  $M$ .

Figure 2.12 shows the far-field optical images obtained on a CCD camera of the polystyrene sample upon white light illumination using a torch.

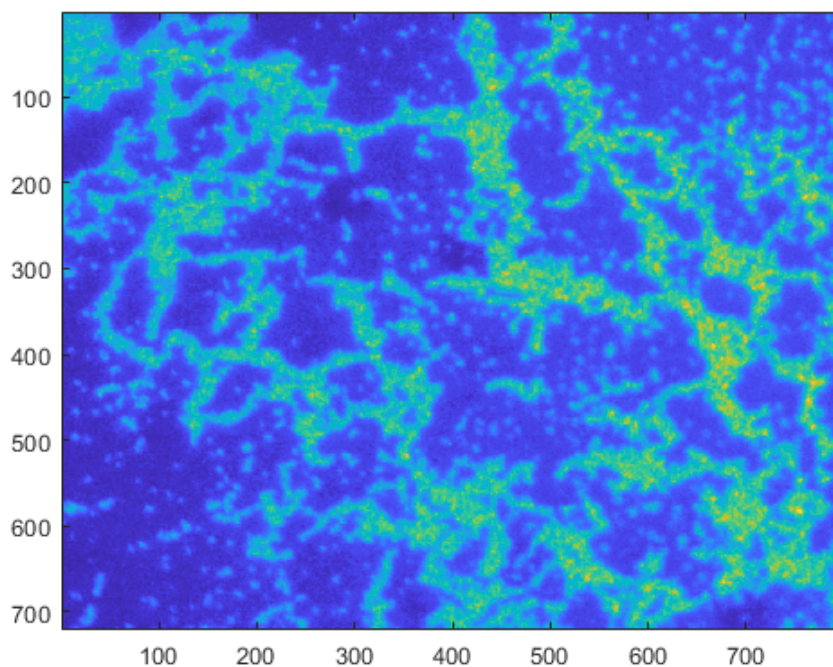


Figure 2.12: Far-field image of polystyrene sample illumination using torch light

Figure 2.13 a) and b) are the far-field images of the polystyrene sample in the same region of interest as Figure 2.12 upon thin fiber loop illumination method and free space illumination method, respectively. It was observed that the  $M$  value obtained was 1.23 for loop illumination and 1.13 for free space method. The high signal to background ratio image from loop illumination method suggests low light scatter in the optical mapping.



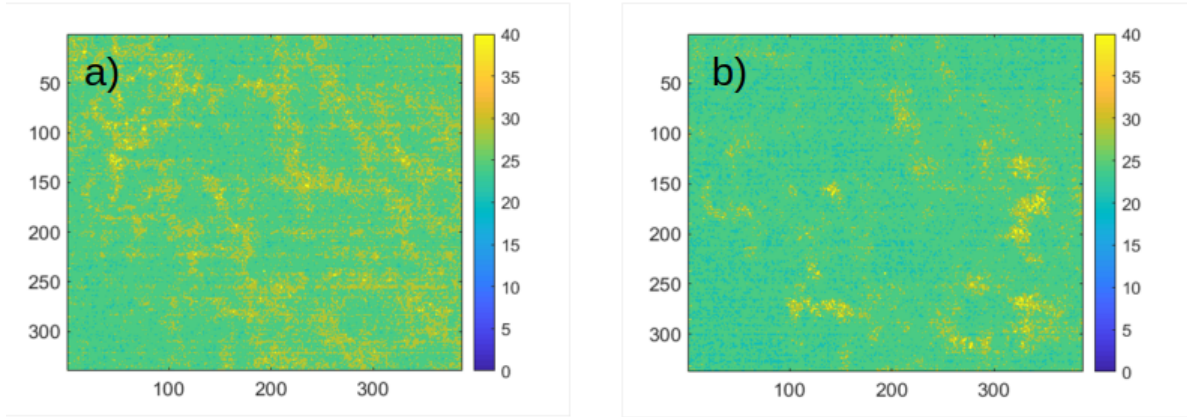


Figure 2.13: Far-field image using a) loop illumination and b) free space coupling



# Chapter 3

## Developing NSOM

A near-field scanning optical microscope(NSOM) is home developed using shear-force as a feedback mechanism [9]. An ultra-sharp fiber tip of few nanometers was pulled using CO<sub>2</sub> laser. The fiber tip probe was glued on to a quartz tuning fork which together formed the NSOM sensing unit. By virtue of damping of oscillatory behaviour of tuning fork based on the shear force exhibited close to the sample, an active feedback mechanism is generated that controls the distance between the tip and sample. Thus, obtaining topography of sample is achieved in tens of nanometer resolution. Using ultra-sensitive photo detectors attainment of optical images is achieved. The chapter reports details and optimization of the indigenously developed NSOM, from making of the tip-probe to obtaining optical images.

### 3.1 Fiber optic probes

As introduced by Prof. Betzig at ATT Bell Labs, we use single mode optical fiber as a probe for our NSOM [10,3]. Thin optical fiber of the order of few tens of nanometers is pulled using a commercial micropipette puller machine. Prior to which the polymer coating on the portion of optical fiber which is meant to be heated by laser, is removed and cleaned with methanol.

The Micropipette puller is used for fabrication of micropipette and optical probes. It works using a CO<sub>2</sub> laser as a heat source and a pulling mechanism. The thin fiber thread making setup(Figure 2.1) is inspired by this framework where instead of breaking the fiber into two, we make a continuous thin thread by varying the heating and pulling parameters. Since the wavelength emitted by the CO<sub>2</sub> laser is in resonance with SiO<sub>2</sub> lattice present in optical fiber, the exposure of fiber to the laser heats it and makes it soft and the puller bars

are drawn apart. After the velocity reaches the set value, the laser turns off and after a specified delay time the hard pull plays on. Thus an optical fiber is pulled in two ultrasharp tips. The tips formed have around 50-100 nm diameter at the ends. SEM images of few tips is shown in Figure 3.1.

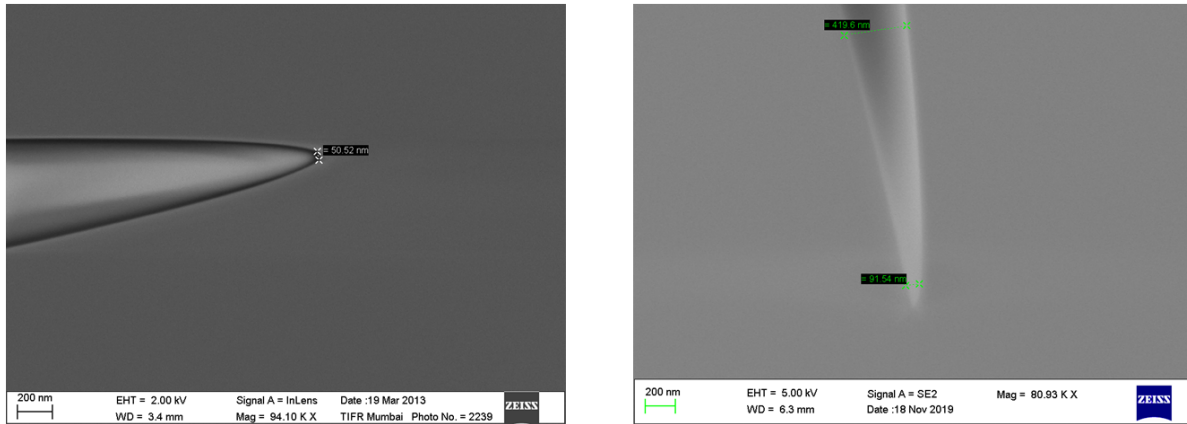


Figure 3.1: SEM of fiber probe tips

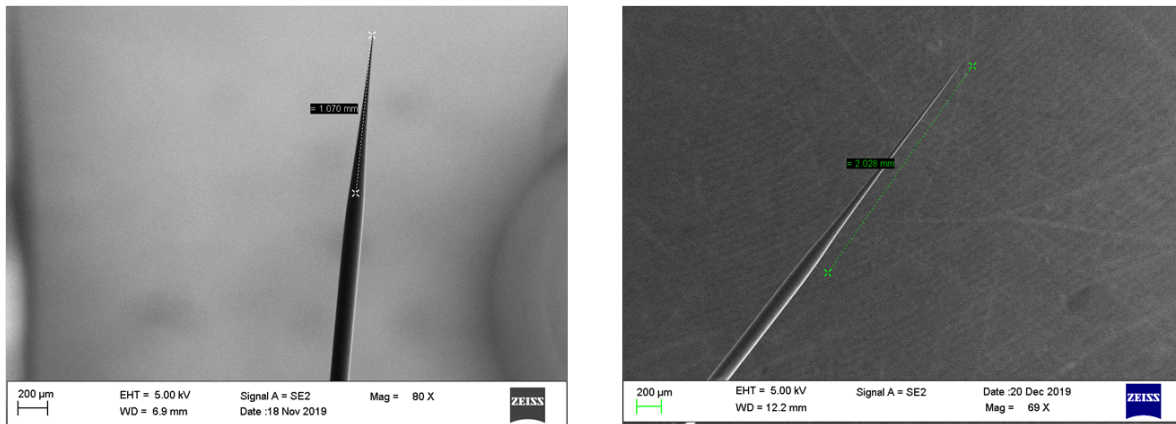


Figure 3.2: SEM of full tapered fiber tips

The entire tapered portion of few fiber tip probes is displayed in Figure 3.2. The puller is programmable to obtain desired configuration of fiber tips by controlling the amount of heat and extent of pulling. The programmable parameters are:

- Heat - The value of actual laser power which varies from 0-10 Watts. Higher the heat, longer and finer the tips formed.

- Fill - Fill or Filament regulates the longitudinal length of fiber to scan and specifies the scanning pattern of laser beams. It varies from 1-8 mm. Increasing fill value will decrease the laser power per unit length equivalent to applying less laser power.
- Velocity - When the speed with which the carrier bars are pulled apart reaches a set velocity value, the laser is turned off. Hard pulling starts after a certain delay time. It is this set velocity value that can be altered. Generally for SiO<sub>2</sub> glass, the value lies in 20-25.
- Pull - The pulling mechanism consists of two pulling forces: a) weak gravity pull as the carrier bars are attached to the cables and b) hard pull produced through passing current through the solenoid coil. Generally, lower pull values produce tips having longer tapered length.
- Delay - It dictates the time between the laser turning off and hard pull activation. If the delay value is too high, the heated portion would cool off before the hard pull is activated resulting into bad tip fabrication.

## 3.2 Shear Force Feedback

The attainment of constant distance of few nanometers between the fiber tip and the sample is regulated by a feedback system based on shear-force detection technique [9]. The shear-force feedback is a non-optical feedback mechanism. As mentioned in section 3.1, the probe is glued on to a quartz tuning fork. An electronic circuit is used to excite the tuning fork. The circuit drives the tuning fork at its resonant frequency, thus making the probe oscillate laterally to the sample surface. Generally at resonance and room temperature, the tuning fork without probe oscillates with an amplitude of 0.3-0.4 pm. At resonant frequency, the amplitude of quartz fork is maximal and generates a voltage which is proportional to the oscillation amplitude. The tip probe experiences a shear force ( $<1\text{nN}$ ) as it approaches the sample leading to change in the oscillating amplitude and change in phase. This change happens mostly close to tens of nanometers, hence this feedback mechanism can be used to maintain fixed probe-sample distance. A schematic of our near-field scanning microscope is shown in the following figure.

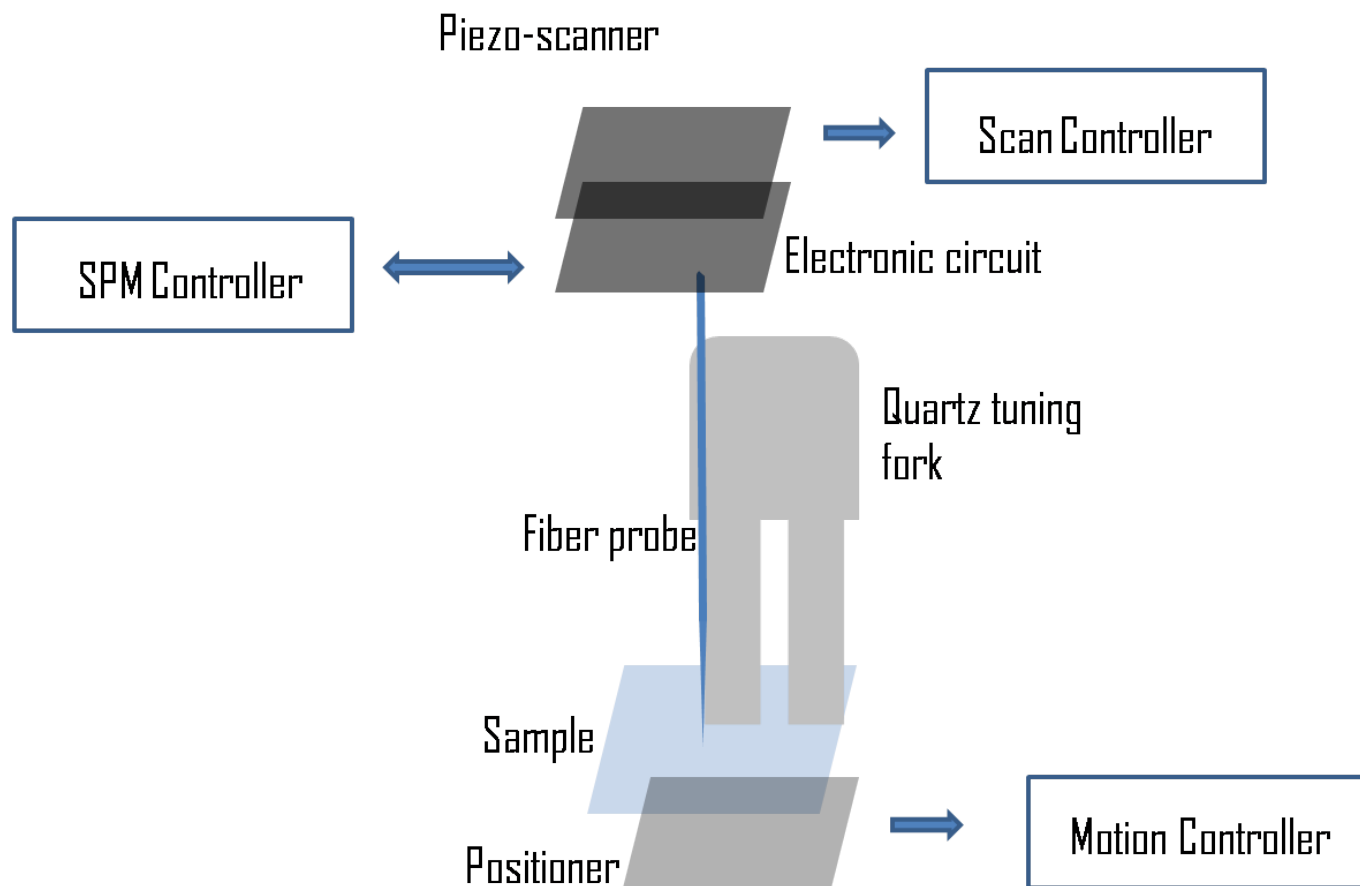


Figure 3.3: Schematic of NSOM

### 3.2.1 Quartz Tuning Fork

Frequency measurements are generally done using the quartz tuning fork owing to its precision, low power consumption and high stability. In scanning probe microscopy, piezoelectric quartz tuning forks were introduced by Gunther, Fischer and Dransfeld [11] and later by Karrai and Grober [12] and others [13,14], as a distance control for NSOM. Quartz can generate electric charge upon exhibition of mechanical stress i.e quartz is a piezoelectric material. Similar to any object, it has its resonance frequency which depends on shape, size, elasticity and speed of sound in it. On applying electric voltage on the crystal we could change its orientation and vice-versa. Hence an electric signal proportional to the applied force is generated. The sensing unit thus if driven at resonance is highly sensitive to sub nN forces present extremely close to the sample. Force detection is carried out by the measurement of fundamental resonance of the sensing unit as a function of applied force. This

is done by electronically driving the unit at resonance voltage and monitoring the induced current. The fiber probes obtained (section 3.1) are then glued on one of the prongs of the tuning fork forming the NSOM sensing unit. One such unit is displayed below.

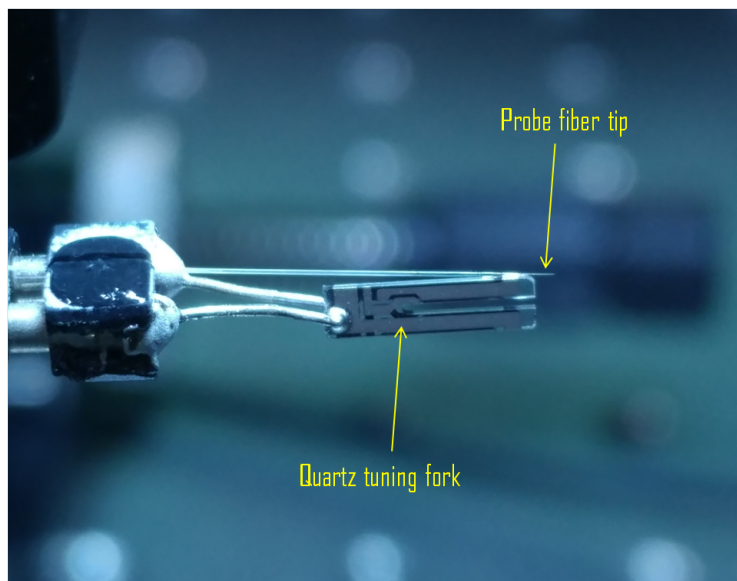


Figure 3.4: NSOM sensing unit: Probe tip glued on quartz tuning fork

### 3.2.2 Electrical model

A series resistor-inductor-capacitor circuit can be used to model all resonators. The RLC Butterworth-Van Dyke model presents electrical analogy to a mechanical damped oscillator, where the acoustic losses are represented by resistors, mass of resonator by inductor and stiffness by capacitor[15]. Our circuit [16] for tuning fork (shown in Figure 3.5) has a capacitance  $C_o$  parallel to the RLC series.  $C_o$  is of the order of few picofarads and is generally known as package resistance. Adding additional capacitance leads to downwards shifting of parallel resonance of crystal. The oscillation frequency of the crystal can hence be varied.

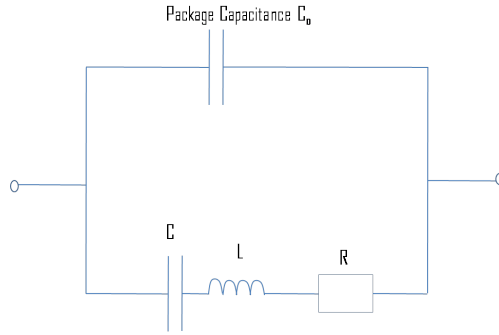


Figure 3.5: Equivalent RLC circuit for quartz oscillator

Induced voltage is measured by driving the tuning fork which makes the probe oscillate using this circuit. The fundamental resonance frequency of the tuning fork is 32.768 kHz. A transformer is used as a voltage source  $V_{in}$  to drive the tuning fork. Both series and parallel resonance is present because of package capacitance. A bridge circuit (shown in Figure 3.6) is used to get rid of package capacitance effect.  $180^\circ$  phase shifted voltage is provided to variable capacitor by the RF transformer. Current through variable capacitor nullifies the current through package capacitance by calibrating the variable capacitor. Hence the circuit acts as a series RLC circuit and the effect is solely due to the quartz resonator. Using an operational amplifier the resulting voltage  $V_{out}$  is measured across the load resistor  $R_g$ . A preamplifier is used to filter and rectify the magnitude of output voltage. The circuit is fixed on a 24 X 24 mm<sup>2</sup> PCB with a voltage source of  $\pm 15V$  for op-amp (Figure 3.7).

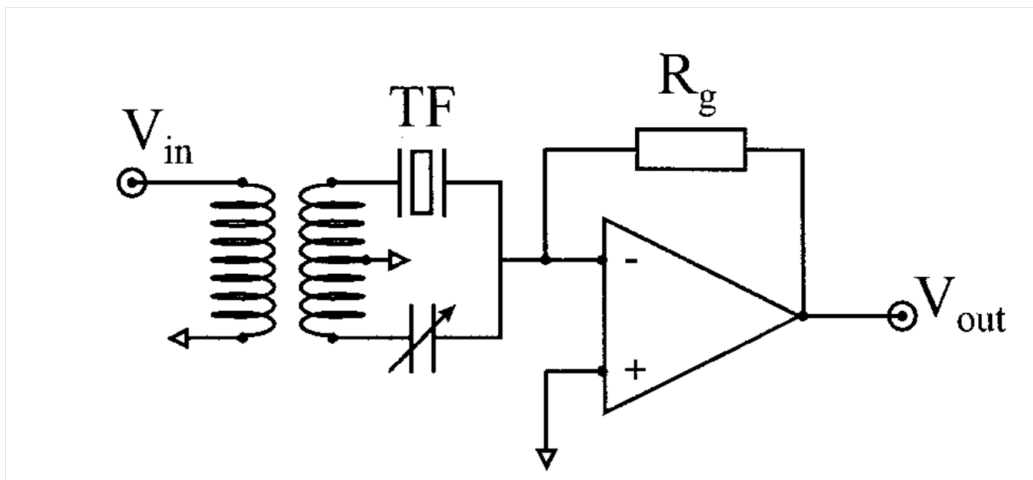


Figure 3.6: Schematic diagram of electronic circuit used in NSOM



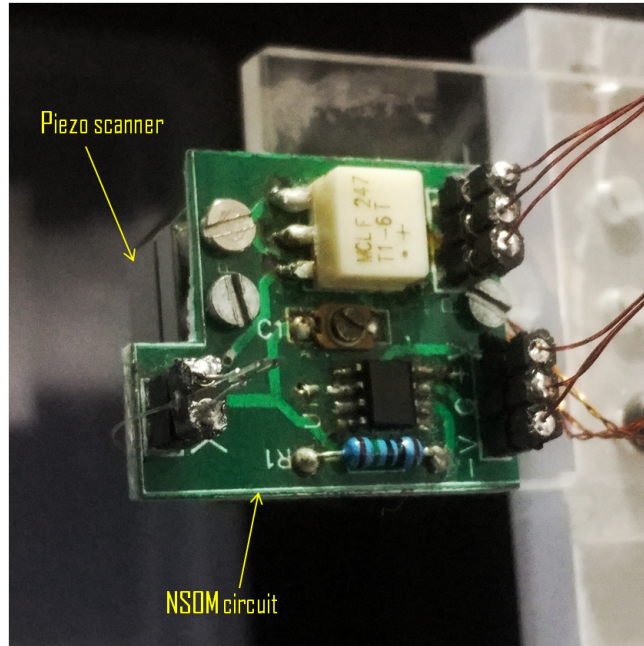


Figure 3.7: NSOM electronic circuit

### 3.2.3 Quality factor

Quality factor or Q-factor describes an oscillating system with resonance. It is a measure of damping and defined as the ratio of energy stored in the resonator to energy loss in each oscillating period. In the circuit, it is the ratio of peak frequency to the full-width half-maximum (fwhm) value i.e  $Q = f_{peak}/f_{fwhm}$ . Determination of sensitivity of the tuning fork is done by the Q factor.  $1/Q$  is proportional to the smallest detectable force. Hence, large quality factor is appreciated for good shear force detection sensitivity. So, high Q implies high frequency stability and accuracy capability of a resonator.

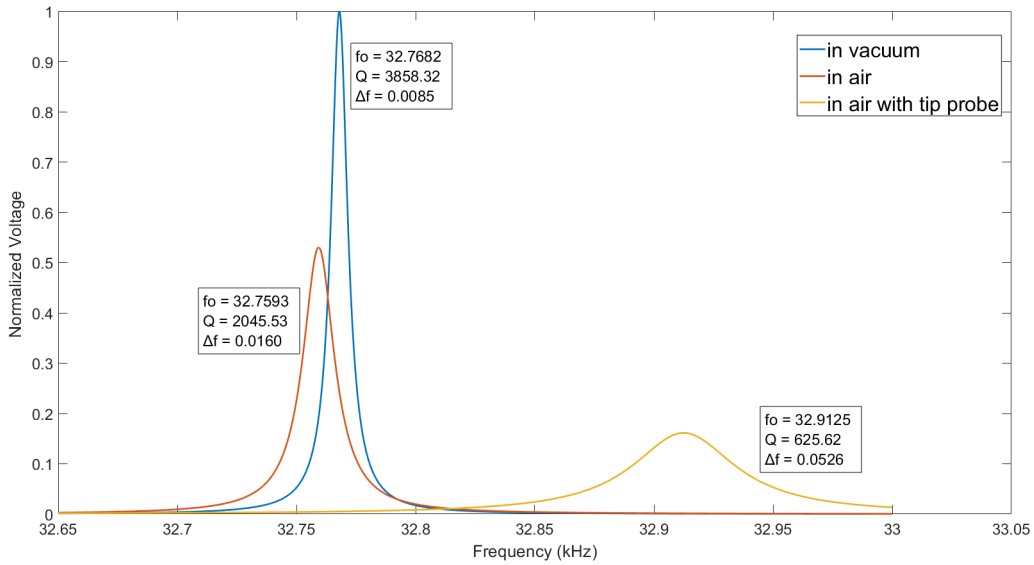


Figure 3.8: Amplitude response of tuning fork resonator in vacuum, in air and with fiber tip glued on it in air.

Figure 3.8 shows the voltage vs frequency plots for tuning fork in vacuum, air and when loaded with fiber probe along with their Q factors. Due to viscous damping of the fork in the air, the Q factor drops down. The right shift in resonance frequency upon loading fiber tip can be attributed to the shift in fundamental mode of the new combined system (fork + tip) from just the fork system. Lorentzian line shape fits the response. The plot also indicates that the package capacitance effect has been nullified and the circuit works as series RLC circuit.

### 3.2.4 Scanner and Positioner

Scanner and positioner are used to take the probe very close to the sample. They both work on the principle of piezoelectric effect, where the translation occurs as a result of expansion or contraction of piezoelectric material upon voltage application. The positioner and scanner are used for coarse and fine adjustment, respectively.

#### Positioner

We are using a 3D nano positioner (Figure 3.9) having motion range of  $80 \mu\text{m}$  per axis. The sample is placed on top of the positioner. The positioner takes the sample close to the probe

tip in the range of motion of scanner. It can be operated manually as well as by triggering it.



Figure 3.9: Nano positioner

## Scanner

The scanner is made up of three piezoelectric stages stacked on each other to give x, y and z degrees of freedom (Figure 3.10). The x and y stages each have  $50 \mu\text{m}$  travel range whereas the z stage has lower travel range of  $24 \mu\text{m}$ . It also works on the same principle of piezo expansions upon voltage application. It is the scanner onto which the the circuit is attached hence the whole sensing unit. So, the approaching of the probe tip is done using the scanner which thereby is controlled by a special electrical controller. The controller is connected to the user interface piezo scan controller which thus drives the piezo scanning stages.

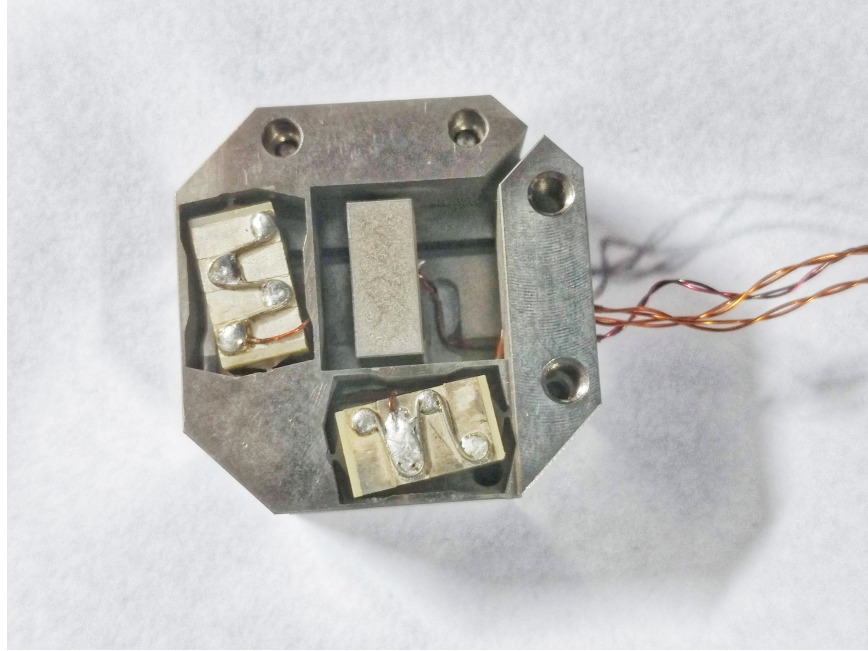


Figure 3.10: Piezo scanner

### 3.2.5 SPM Controller and Software

Controlling the scan position and scanner movement is done by the SPM controller and software. It also acquires several signals simultaneously and saves the scanned images. The voltage required ( $\pm 15$  V) and input signal is also provided by the controller and software.

### 3.2.6 Calibration

Characterization of the resonance frequency and phase response of the sensing unit is done using SPM controller and software. Collection of response for the phase and amplitude is done by sweeping frequency. Using the calibration feature in the software the Q factor can be measured. From the amplitude vs frequency plot, FWHM and peak frequency is calculated. Hence Q factor is calculated using the formula:

$$Q = \frac{f_{peak}}{\Delta f} \quad (3.1)$$

Figure 3.11 shows the calibration amplitude and phase response. The frequency is swept from 30-35 kHz. The peak in amplitude occurs at the resonance frequency of the sensing unit.

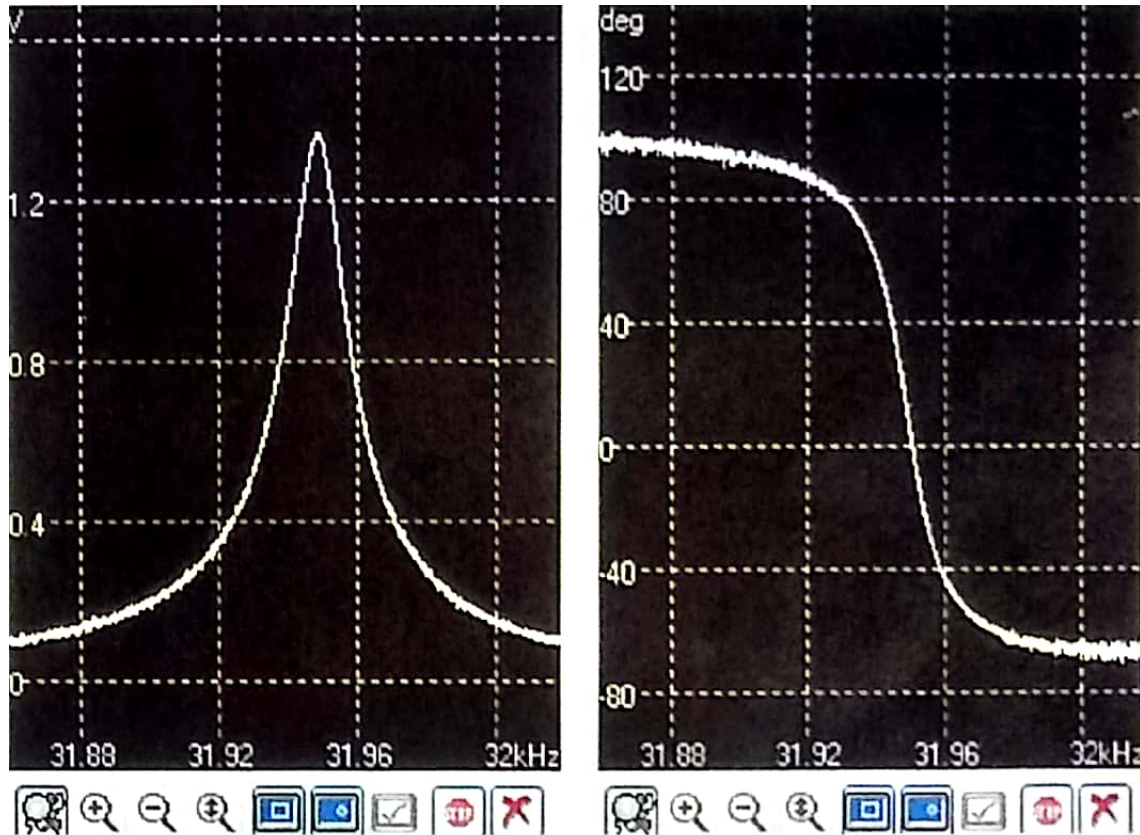


Figure 3.11: Amplitude and Phase response of the resonator

### 3.2.7 Locking of probe

Once the calibration is done, the excitation frequency is set equal to the resonance frequency using the calibration plot. The offset phase is also set to 0 at the resonant frequency. Next stage is to lock the fiber probe tip at a constant distance few tens of nanometers from the sample. This can be done in two ways:

#### Amplitude modulation mode

Driving the z controller and gaining topographic information is done by determining the change in oscillation amplitude by driving the tuning fork at a fixed frequency. In this mode, the oscillator (tuning fork or cantilever) is continuously excited at the resonance frequency  $f_0$ , i.e the resonant frequency of the oscillator in air. Figure 3.12 shows the amplitude response in the presence of force gradient and the red dots shows the working point for amplitude modulation mode locking.

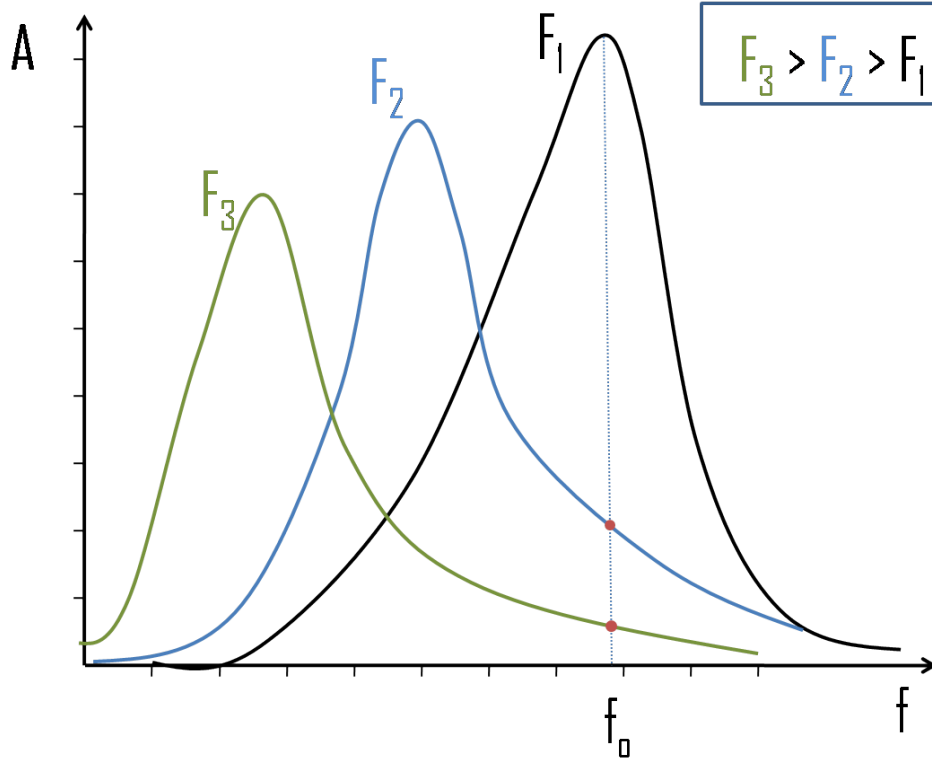


Figure 3.12: Working points in amplitude modulation mode (Red dots)

### Phase locked loop

Phase locked loop or PLL mode is used to control high Q factor oscillators like in the case of low temperature oscillators. This method uses the fact that the phase shift at resonance between the input and output signals is  $\pi/2$ . The excitation frequency is controlled in this mode. To keep the excitation in resonance, a proportional integral control loop is used. The phase between excitation and oscillation signal is the input to this loop and excitation frequency or the shift in excitation frequency  $\Delta f$  is the output for this loop. The force gradient affecting the oscillation is directly proportional to the frequency shift  $\Delta f$ . Figure 3.13 shows the PLL operation mode where the green dots are the working points. The input of the z controller is the output of phase loop to keep the frequency shift and hence the force on the probe tip constant.

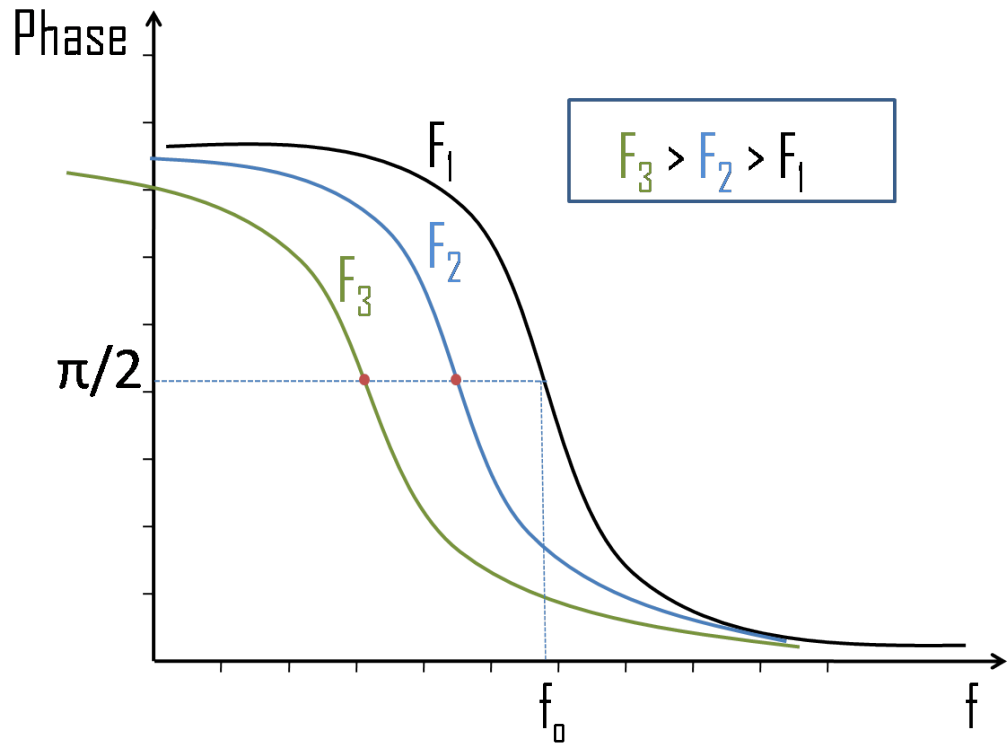


Figure 3.13: Working points in PLL mode (Red dots)





# Chapter 4

## Investigation of NSOM and loop illumination

Since the NSOM optimization and calibration is done, we test the NSOM by obtaining near-field topography and near-field optical scans. The phase locked loop (PLL) method was used for probe locking on the samples. The topographical test scans were obtained on AFM calibration samples, 2D photonic crystal waveguide sample and NSOM test grating samples. The optical test scans were obtained by recording the evanescence of interference pattern formed in the prism. Non-linear behaviour of piezo-scanner through which the probe movements are controlled were observed. This type of discrepancy primarily arises from changing environmental conditions such as humidity and temperature. Thus, every now and then the piezo scanner requires re-calibration and is a routine process. This non-linearity hampers the scan obtaining ability to acquire fine structure topographies of photonic crystals. Near-field optical scans of NSOM calibration sample was obtained by thin fiber loop illumination and free space illumination. Quantification of better source of illumination was done by comparing the two illumination method by measuring the signal to background ratio.

### 4.1 Topographical scans

Various samples were tested for obtaining the topography in NSOM.

### 4.1.1 AFM calibration samples

The AFM sample were the height standards fabricated to exhibit high quality calibration standards. The sample features silicon dioxide ( $\text{SiO}_2$ ) on a 5 X 5 mm silicon chip and the step height is around 100 nm. The chip consists of different geometry and pitch as shown in Figure 4.1.

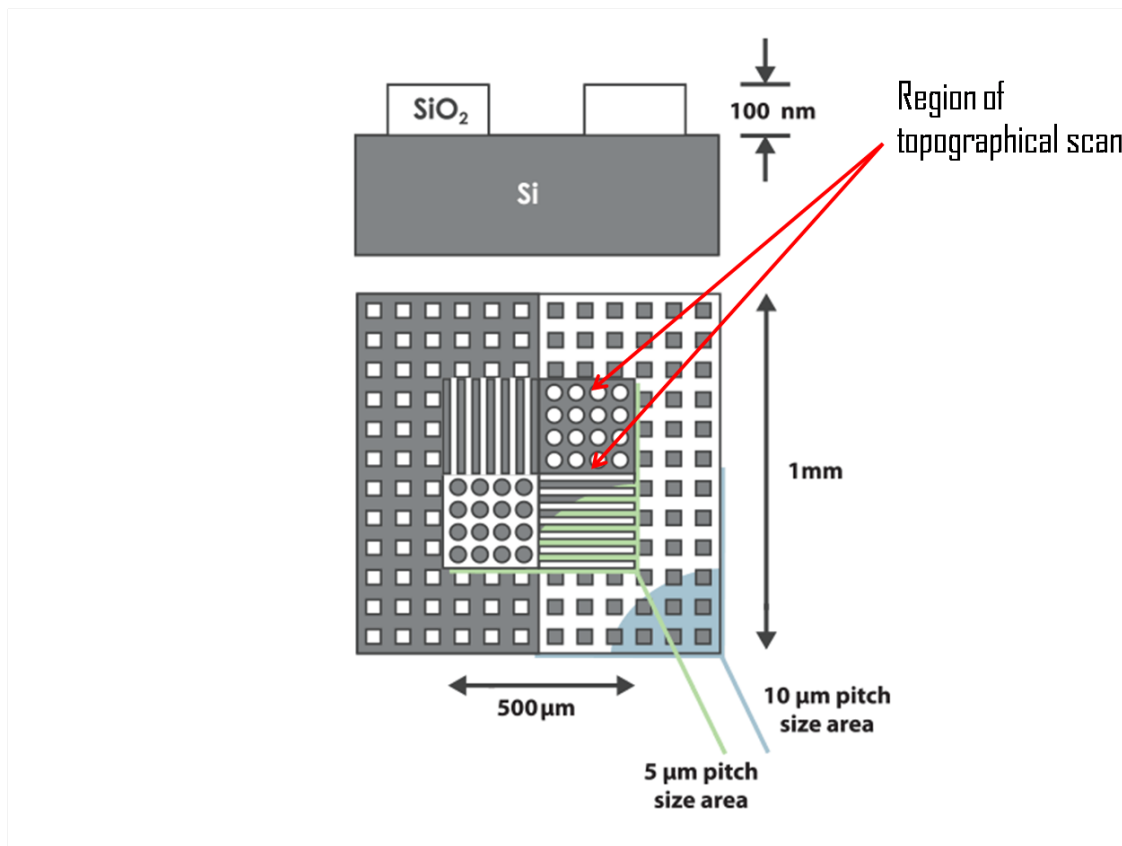


Figure 4.1: Schematic of AFM calibration sample

The region of interest chosen for the topographical scans was circular  $\text{SiO}_2$  pillars, as depicted in the figure. Following is the topographical scans obtained.

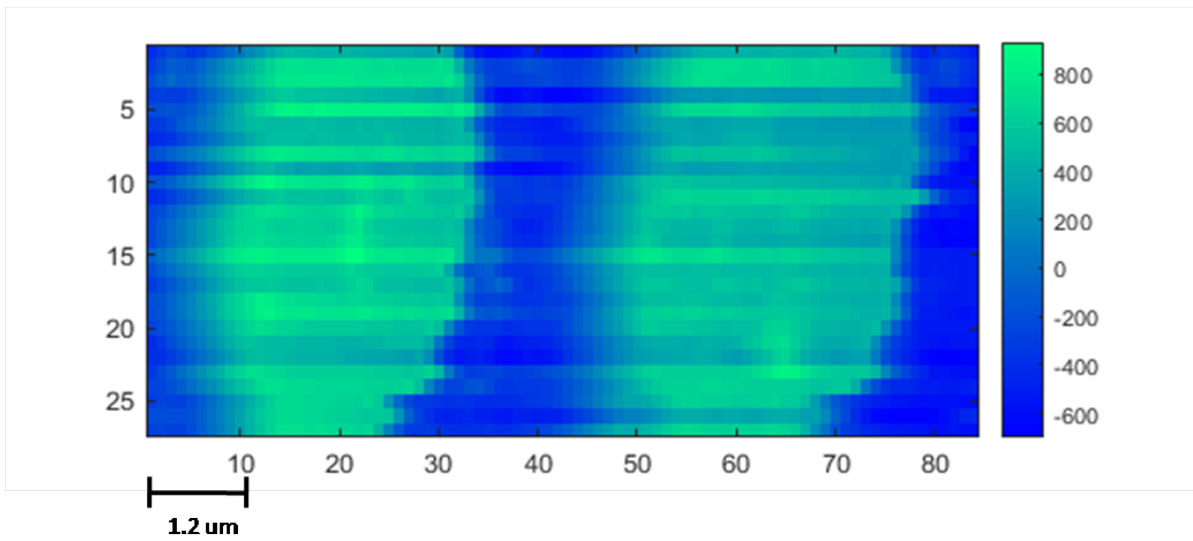
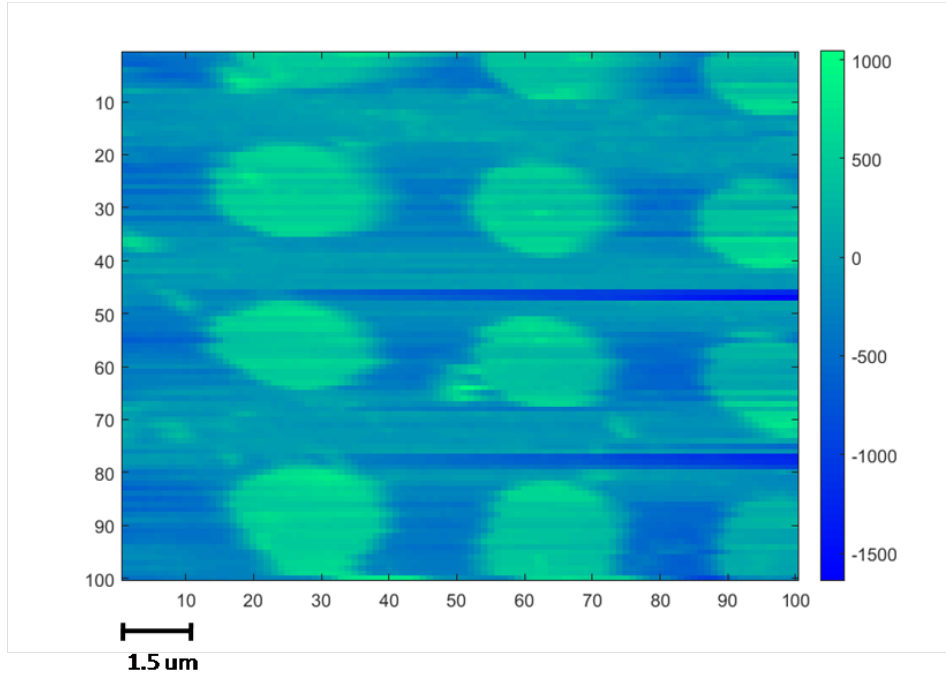


Figure 4.2: Near-field topography of AFM calibration sample

#### 4.1.2 Photonic crystal waveguide samples

A photonic crystal consists of periodic nano-structures that interacts with photons affecting it similar to the way an electron gets affected by periodic potential in a crystal lattice. It can be fabricated by periodic arrangement of materials having different dielectric constants. The photonic crystal we had is a periodic structure of air holes in gallium arsenide membrane.

The waveguide is formed by letting an array of holes absent in the structure. The Scanning electron microscope images of the waveguides is shown in Figure 4.3.

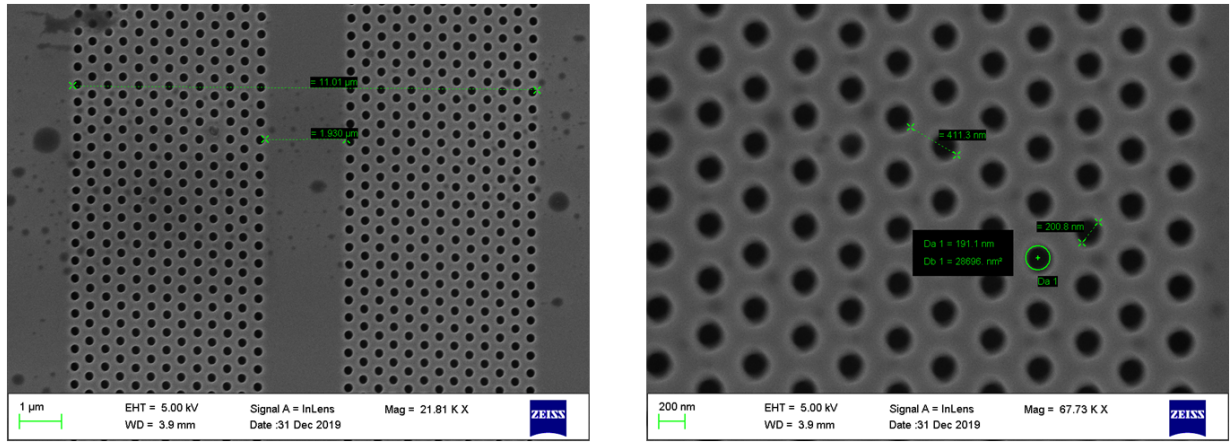


Figure 4.3: Photonic crystal waveguide

Non-linear shift in the hole locations was observed in the near-field topographical scans of the waveguide samples. This shift can be attributed to improper calibration of the piezo-scanners controlling the scanning motion of the NSOM probe due to environmental changes such as in humidity and temperature. One such topographical scan exhibiting non-linear shift is shown in Figure 4.4.

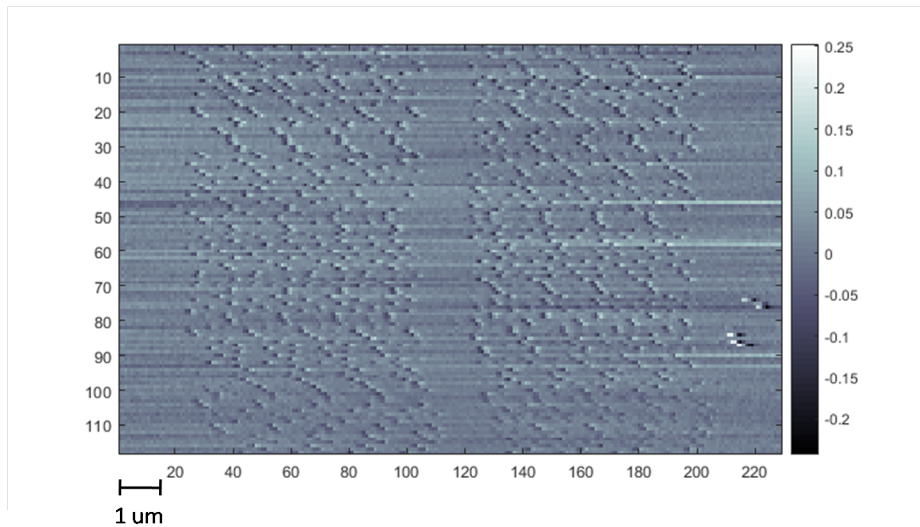


Figure 4.4: NSOM topography of photonic crystal waveguide

### 4.1.3 NSOM test grating

These are test grating using near-field optical detection in microscopy. It consists of vanadium rhombus on 10X10 mm quartz substrate, the schematic is shown in Figure 4.5 . The structure step height is of the range 20 - 30 nm.

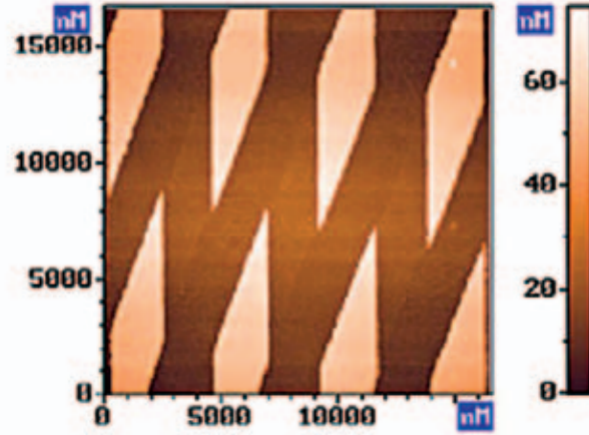


Figure 4.5: Schematic of test grating

SEM images of the gratings is shown in the following figure. It was observed that major sections of these rhombus were broken or had fallen off. Hence this grating would be model in obtaining near-field optical signals as it contains segments of vanadium scatterers on quartz substrate.

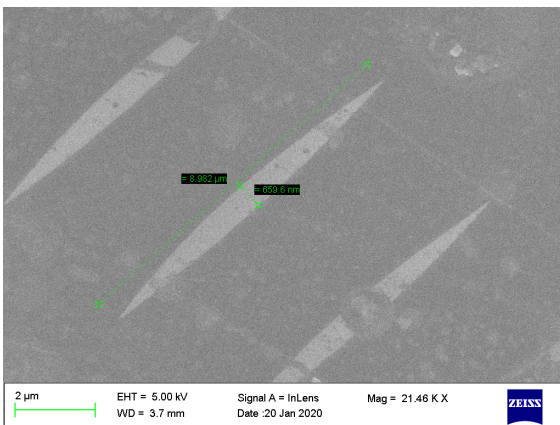


Figure 4.6: SEM of Vanadium Rhombus

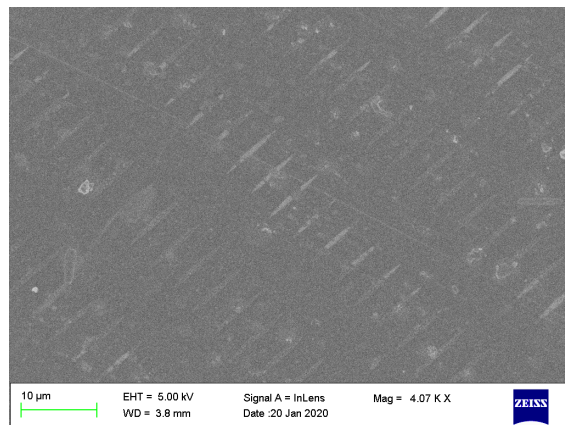


Figure 4.7: SEM of grating

Near-field topography of two such test grating rhombus is shown in Figure 4.8.

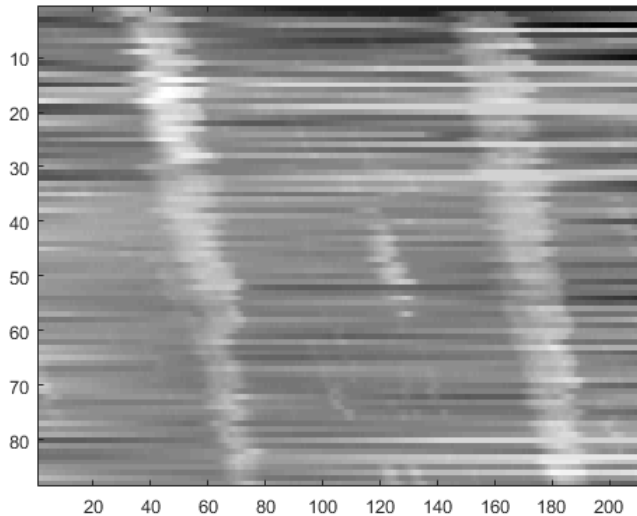


Figure 4.8: Near-field topography of test grating

## 4.2 Optical scans

In the previous section we successfully accomplished the calibration and attainment of topographical scans and locking the NSOM probe onto samples retaining nanometer step ranges. This section investigates the near field optical signature and authenticates the evanescence nature of NSOM. We recorded an optical map of evanescence from an interference pattern formed when two counter propagating beams were made to undergo total internal reflection(TIR) at the glass-air interface in a prism. The experimental setup for the same is shown in Figure 4.9. A 630 nm He-Ne laser beam is allowed to undergo TIR at the hypotenuse face of a right-angle prism. The beam is reflected back tracing the same path as incident beam using a dielectric mirror. The light captured by the NSOM optical fiber probe is detected by an ultra-sensitive few photon detector which further is connected to the SPM controller.

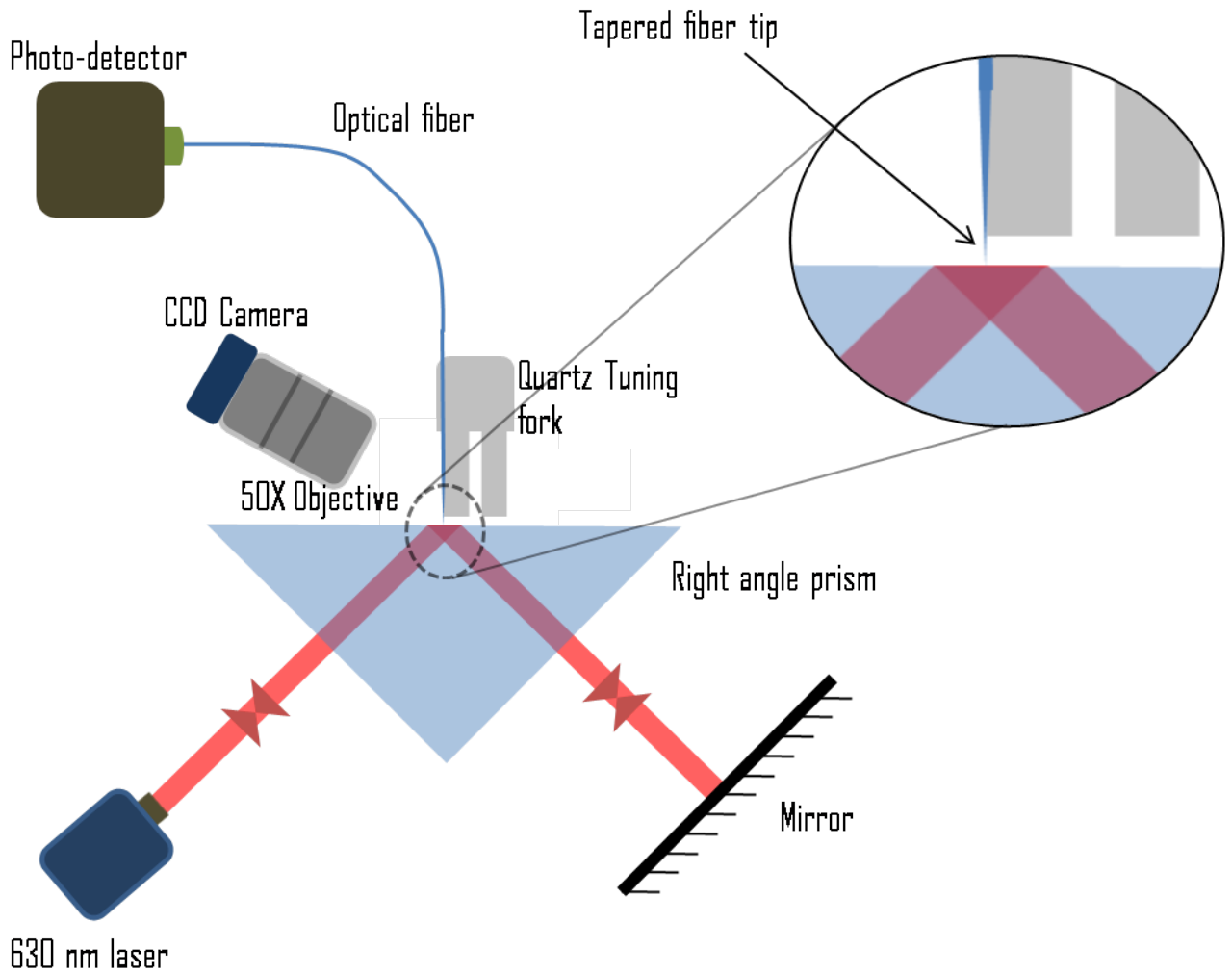


Figure 4.9: Schematic of experimental setup to map near-field interference pattern

The near-field optical map thus recorded is also an interference pattern as shown in Figure 4.10. This interference map results from the evanescence of bright and dark fringes formed inside the prism by the two counter propagating beams at the TIR intersection of the hypotenuse face. To confirm its evanescence nature, we performed a scan by keeping the probe-sample distance much greater than penetration depth of the evanescent waves (around  $2\mu\text{m}$ ). The optical scans thus obtained did not show any interference pattern. Hence, this experiment exhibits an absolute evanescent nature of NSOM and its limitless scientific application.

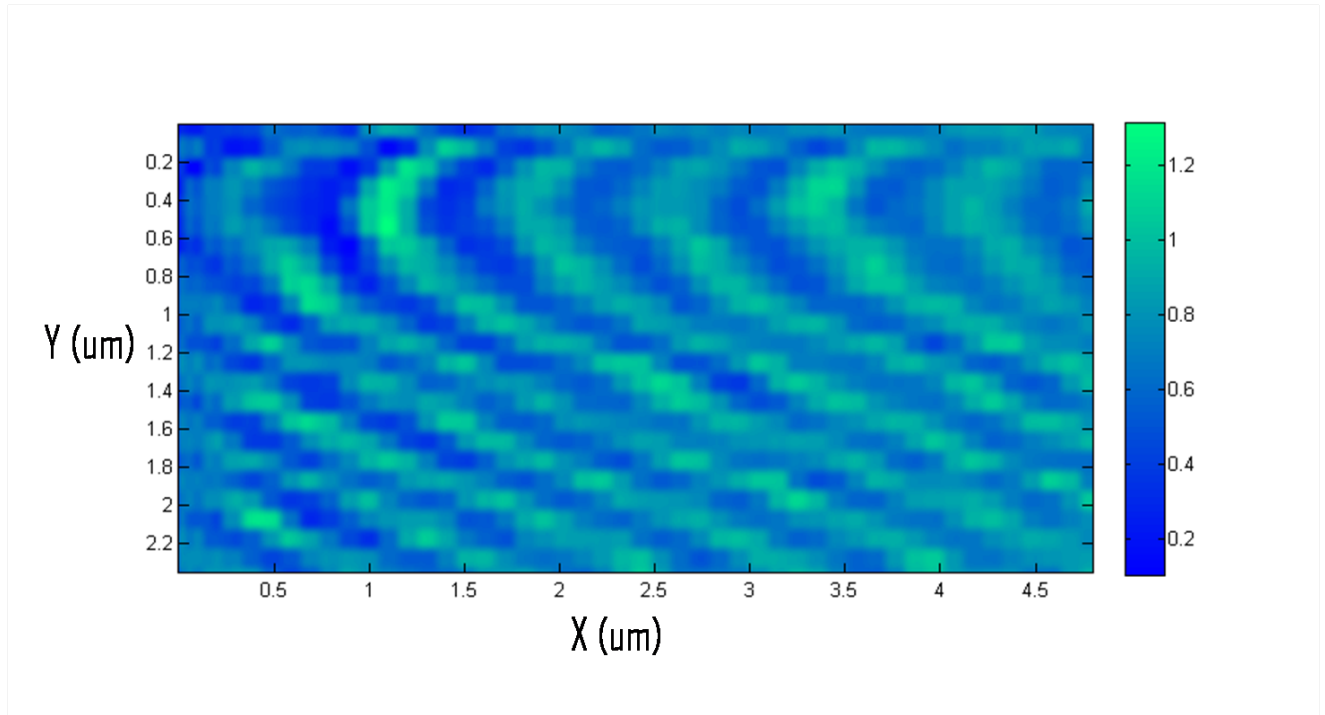


Figure 4.10: Near field evanescence of interference pattern

### 4.3 Loop illumination

Now that the assemblage and calibration of indigenous NSOM is done, we performed qualitative scans to compare the two methods of illumination. Near-field scans of an optical calibration sample and an optical scan for probe-sample distance of  $2 \mu m$  on scotch tape sample was carried out. Figure 4.11 depicts the schematic of the experimental setup for thin fiber loop and free space coupling method.



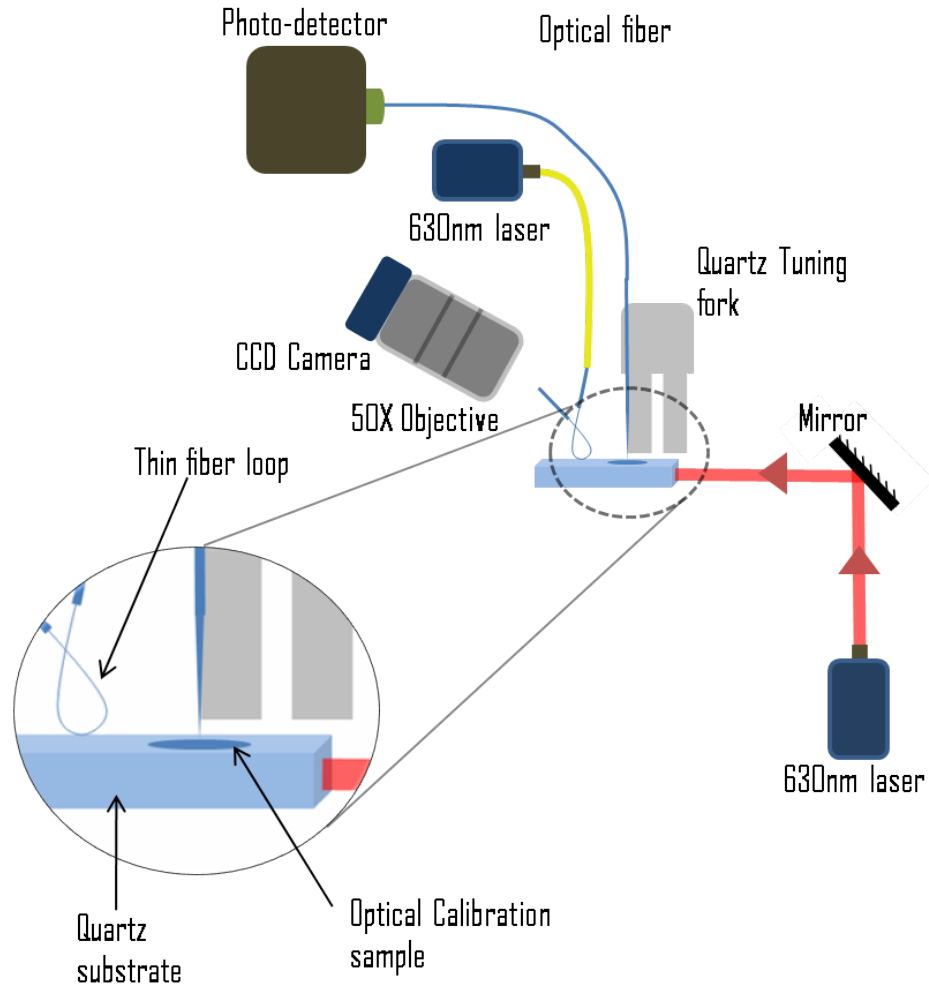


Figure 4.11: Schematic for thin fiber loop and free space coupling in near-field.

### 4.3.1 Vanadium on quartz substrate sample

Simultaneous topographical and optical measurements were obtained for excitation using both methods. Near-field topography and optical maps by both methods for vanadium sample on quartz substrate (Figure 4.12). As usual, light was coupled into the quartz substrate. It was observed that the measure of improvement,  $M$  (the ratio between intensity at the sample region to the background) is greater for the loop illumination method (i.e.,  $M = 1.46$ ) than the free space coupling method (i.e.,  $M = 1.19$ ).

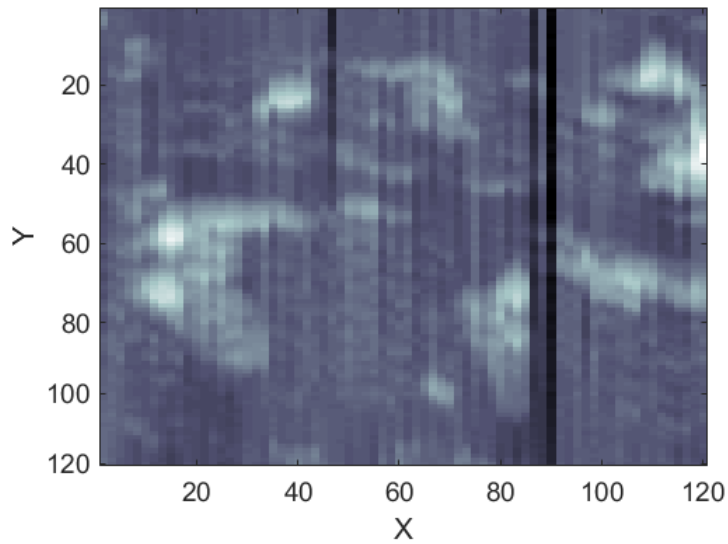


Figure 4.12: Topography of the raster scanned region

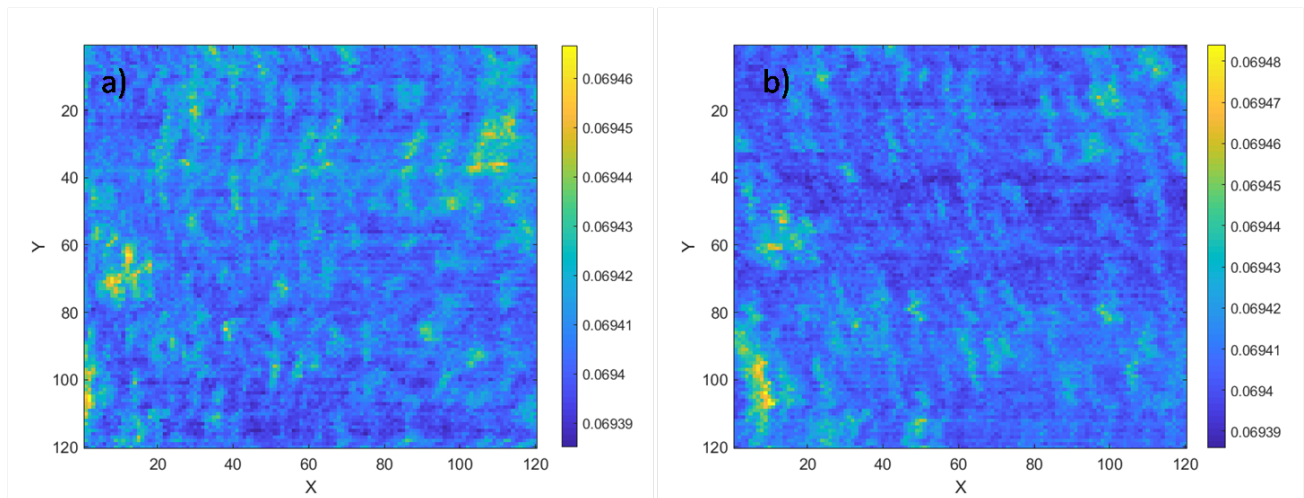


Figure 4.13: Near-field optical scan by a) loop illumination and b) free space coupling.

### 4.3.2 Scotch tape on glass slide sample

Since the locking of NSOM probe on scotch tape sample is unfeasible, an optical map was obtained by keeping the probe-sample distance  $2 \mu\text{m}$  apart. The excitation was done using both the methods of illumination. A similar setup of Figure 4.11 was implemented to carry this experiment. The measure of scatter is considered to be the speckle contrast,  $C$  defined as the ratio of fluctuation in measured intensity to the mean intensity value. Higher  $C$  value

of 0.52 was recorded for the loop coupling excitation than for free space coupling( $C = 0.48$ ). The optical mapping for both cases are shown in the following figures.

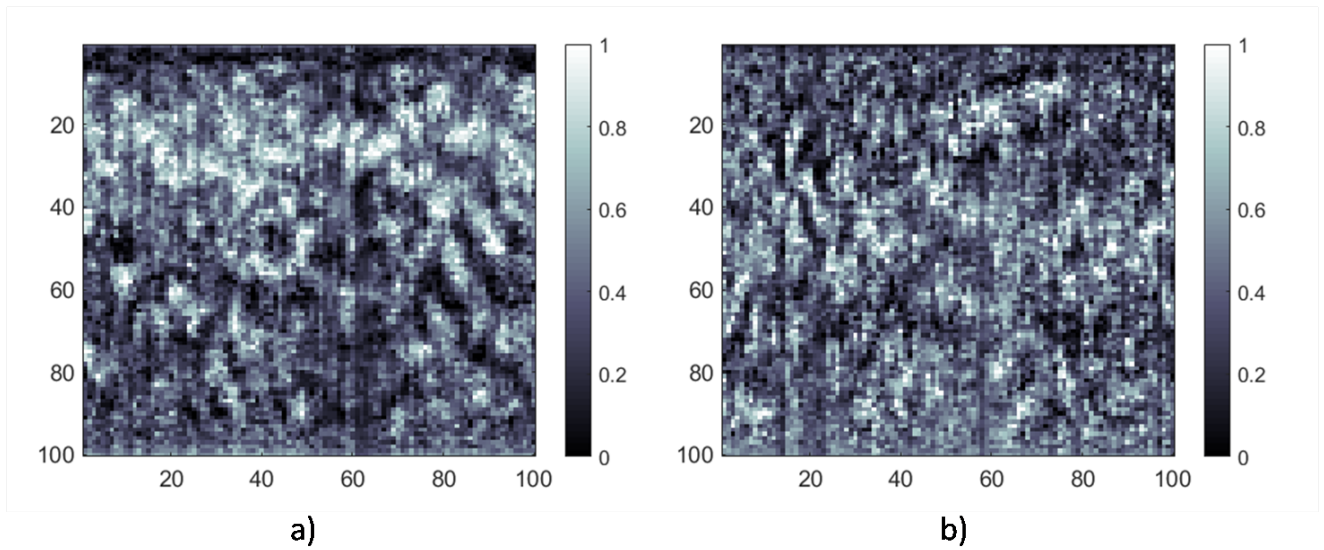


Figure 4.14: Speckle pattern obtained on scotch tape sample by a) loop illumination and b) free space coupling method.

Hence, it is concluded that the evanescence coupling using thin fiber loop is an effective method leading to high signal to noise ratio and high contrast compared to the free space coupling method.



# Chapter 5

## Conclusion and Further Outlook

Near-field studies concede access to crucial high wave vector spatial information which otherwise is inaccessible through the conventional far-field studies. An indigenous near-field scanning optical microscope (NSOM) was assembled and calibrated to serve this purpose. A key element in NSOM is the excitation of the sample. Conventional free space excitation of NSOM sample comes with the demerit of unwanted scatter leading to bad contrast and low signal to noise ratio. To overcome this drawback, a source of evanescent light was designed.

Light propagation in an optical fiber occurs as a result of total internal reflection (TIR) at its core-cladding interface. The fact that evanescent waves are generated in the rarer medium (cladding in optical fiber) at the TIR interface was used as an evanescence source. However the cladding limits its accessibility as the thickness of cladding is much greater than the penetration depth of evanescent wave. An experimental setup was designed to obtain very thin optical fiber thread of around  $10\ \mu\text{m}$  thickness. To obtain the thin fiber thread, simultaneous melting and stretching of optical fiber using  $\text{CO}_2$  laser and motorized translational stage, respectively was implemented. Although the thickness of fiber thread was not constant throughout the fiber thread, effective propagation of light with low losses was observed. The inconstant thickness could be improved by upgrading the setup to make the fiber stretch from both ends instead of one.

A small loop of around 3 mm was made from the thin fiber thread, allowing access to a set of evanescent waves in various direction tangential to the loop. The test for evanescence was conducted by designing an experiment to couple the evanescent waves from loop into a glass slide on one end and observing illumination of sample placed at the other end in far-field. The sudden appearance and disappearance of optical signature when the loop is taken closer and away respectively from the slide indicated the successful coupling of evanescent

light into the glass slide.

Evanescent light coupling using thin fiber loop was achieved on various samples and was observed in far-field and near-field. Far-field measurements were obtained for samples like scotch tape and polystyrene on glass slide using 630 nm excitation and scribbled structure on silicon wafer using 1.5  $\mu\text{m}$ . Successful evanescent coupling were observed. Near-field measurements were made on vanadium structure deposited on quartz substrate. It was observed that the locking on NSOM probe on few samples such as glass or scotch tape is unfeasible. This can be attributed to weak shear force exhibition by the sample. Qualitative comparison of thin fiber loop coupling and free space coupling method was done using far and near field measurements. Evanescent coupled light excitation proved to produce high contrast optical signals in each independent study of the samples in far and near field measurement. Thus it is concluded that indeed the loop illumination method surpasses the conventional free space coupling method as an excitation source.

The next phase of the project is to use this newly developed evanescent source to excite the 2-dimensional photonic crystal samples. Various mesoscopic phenomena such as diffusion, weak localization and Anderson localization of light can be systematically studied in these disordered 2D photonic crystals. By implementing the thin fiber loop excitation technique, the demerit of unwanted scatter arising from the conventionally used free space coupling excitation could be overcome. Hence, by integrating the fiber loop excitation method in NSOM we would be able to study light transport in the disordered 2D PhC samples. Near-field optical measurements could then be undertaken to study phenomena such as mode profiles, conductance, Anderson localization, intensity statistics, multifractality, etc.

# Bibliography

- [1] D. W. Pohl, W. Denk, and M. Lanz, *Appl. Phys. Lett.* 44, 651 (1984).
- [2] U. Durig, D.W. Pohl and F. Rohner, *Journal of applied physics*, 59(10), 3318-3327(1986).
- [3] E.J. Betzig, J.K. Trautman, T.D. Harris, J.S. Weiner, R.L. Kostelak, *Science* 251 (5000),1468-1470(1991).
- [4] E.H. Synge: *Philos. Mag.* 6, 356 (1928)
- [5] E. Abbe: *Arch. Miroskop. Anat.* 9, 413 (1873)
- [6] Lord Rayleigh, "On the theory of optical images with special reference to the microscope," *Philos. Mag.* 5(42), 167-195 (1896).
- [7] J. M. Vigoureux and D. Courjon, *Detection of nonradiative fields in light of the Heisenberg uncertainty principle and the Rayleigh criterion*, *Appl. Opt.* 31, 3170-3177 (1992)
- [8] L. Novotny, *The History of Near-field Optics*, *Progress in Optics* 50, E. Wolf (ed.), chapter 5, p.137- 184 (Elsevier, Amsterdam, The Netherlands, 2007).
- [9] E. Betzig, P.L. Finn, S.J. Weiner: *Appl. Phys. Lett.* 60, 2484 (1992)
- [10] E. Betzig: In *Near-Field Optics*, ed. by D.W. Pohl, D. Courjon, NATO ASI Ser. E, Vol. 242 (Kluwer, Dordrecht 1993) p. 7
- [11] P. Gunther, U. Ch. Fischer, and K. Dransfeld. *Scanning near-field acoustic microscopy.*, *Applied Physics B*, 48:89–92, 1989.
- [12] K. Karrai and Robert Grober, *Piezoelectric tip-sample distance control for near field optical microscopes.*, *Appl. Phys. Lett.*, 66(14):1842–1844, April 1995.
- [13] A. G. Ruiter, J. A. Veerman, K. O. van der Werf, and N. F. van Hulst, *Dynamic behavior of tuning fork shear-force feedback.*, *Appl. Phys. Lett.*, 71(1):28–30, (July 1997).
- [14] A. G. T. Ruiter, J. A. Veerman K. O. van der Werf, M. F. Garcia-Parajo, W. H. J. Rensen, and N. F. van Hulst, *Tuning fork shear-force feedback. Ultramicroscopy.*, 71:149–157 (1998).

- [15] Domarkas V, Kazys R-J. editors. *Piezoelectric transducers for measuring devices.*, Vilnius: Mintis, (1975).
- [16] Grober, Robert Acimovic, Jason Schuck, Jim Hessman, Dan Kindlemann, Peter Hespanha, Joao Morse, A. Karrai, Khaled Tiemann, Ingo Manus, Stephan. *Fundamental limits to force detection using quartz tuning forks*, Review of Scientific Instruments. 71. 2776-2780. 10.1063/1.1150691 (2000).